Int Journ Earth Sciences (1999) 88:513–531

ORIGINAL PAPER

A. Kilias · G. Falalakis · D. Mountrakis

Cretaceous–Tertiary structures and kinematics of the Serbomacedonian metamorphic rocks and their relation to the exhumation of the Hellenic hinterland (Macedonia, Greece)

Received: 8 December 1998 / Accepted: 19 April 1999

Abstract The kinematic pattern and associated metamorphism of the predominant ductile deformation and the subsequent deformational stages of the Serbomacedonian metamorphic rocks and granitoids are presented in terms of peri-Tethyan tectonics. A systematic record of structural and metamorphic data gives evidence of a main top-to-ENE to ESE ductile flow of Cretaceous age (120–90 Ma) associated with a crustal stretching and unroofing. A subordinate WSW to WNW antithetic sense of movement of the tectonic top is observed in places. The associated metamorphic conditions are estimated at 4.5–7.5 kbar and 510–580 °C. During Eocene to Miocene times these fabrics were successively deformed by low-angle extensional D_e ductile shear zones with top-to-NE and SW sense of movement and brittle shear zones of similar kinematic pattern, suggesting a transition from ductile to brittle deformation. D_e deformation was accompanied during its later stages by NW/SE-directed shortening. We also discuss the relation of this Cretaceous–Tertiary deformation of the Serbomacedonian metamorphic rocks with the Eocene to Miocene ductile, top-to-southwestward crustal shear of the adjacent Rhodope crystalline rocks. We regard the Serbomacedonian and the Rhodope metamorphic rocks to represent related metamorphic provinces, the most recent exhumation and cooling history of which is bracketed between the Eocene and Neogene.

Key words Serbomacedonian · Rhodope · Deformation · Cretaceous · Tertiary· extension · Exhumation · Moesian · Shear-sense

A. Kilias (✉) · G. Falalakis · D. Mountrakis
Department of Geology and Physical Geography,
School of Geology, Aristotle University of Thessaloniki,
GR-54006 Thessaloniki, Greece

Introduction

The Serbomacedonian massif (SRB) of northern Greece is the southern continuation of metamorphic rocks outcropping in southwestern Bulgaria and southeastern former Yugoslavia. It belongs to the Hellenic hinterland and has a complicated tectonic structure with a heterogeneous mix of metamorphic lithological units of Palaeozoic or older age, intruded by Mesozoic and Cenozoic granitoids (Dimitrijeviè and Ciriè 1966; Kockel et al. 1971, 1977; Jacobshagen et al. 1978; Sakellariou 1989; Chatzidimitriadis et al. 1985; De Wet et al. 1989; Sidiropoulos 1991; Kourou 1991).

To the west, the SRB tectonically borders chiefly Mesozoic metasediments and magmatic rocks of the Circum-Rhodope belt (Kauffman et al. 1976; Kockel et al. 1977). Still farther west, ophiolitic rocks of the Axios zone extend along the western border of the Circum-Rhodope belt, forming obducted remnants of the Jurassic Axios ocean (Fig. 1; Mercier 1968; Mercier et al. 1975; Jacobshagen et al. 1978; Vergely 1984). To the east the SRB lies structurally above the Pangaio unit of the Rhodope crystalline rocks (Kockel and Walther 1965; Kronberg et al. 1970; Koukouzas 1972; Dinter and Royden 1993; Sokoutis et al. 1993).

Investigations have thus far failed to throw much light on the overall tectonometamorphic history and kinematics of the SRB, or on the role it played in the Alpine tectonic evolution of the Hellenic hinterland and the southern Balkan peninsula. We envisaged that the study of the predominant ductile deformation and the subsequent deformational events, pervasively imprinted throughout the SRB, would advance our understanding of the structural evolution of the SRB and help to determine its setting in the tectonic evolution of the Eastern Mediterranean area.

In this paper we present a detailed study of the predominant ductile deformation and the subsequent deformational stages of the Serbomacedonian metamorphic rocks. Our investigations are based on field observations, geothermobarometric estimates and kine-

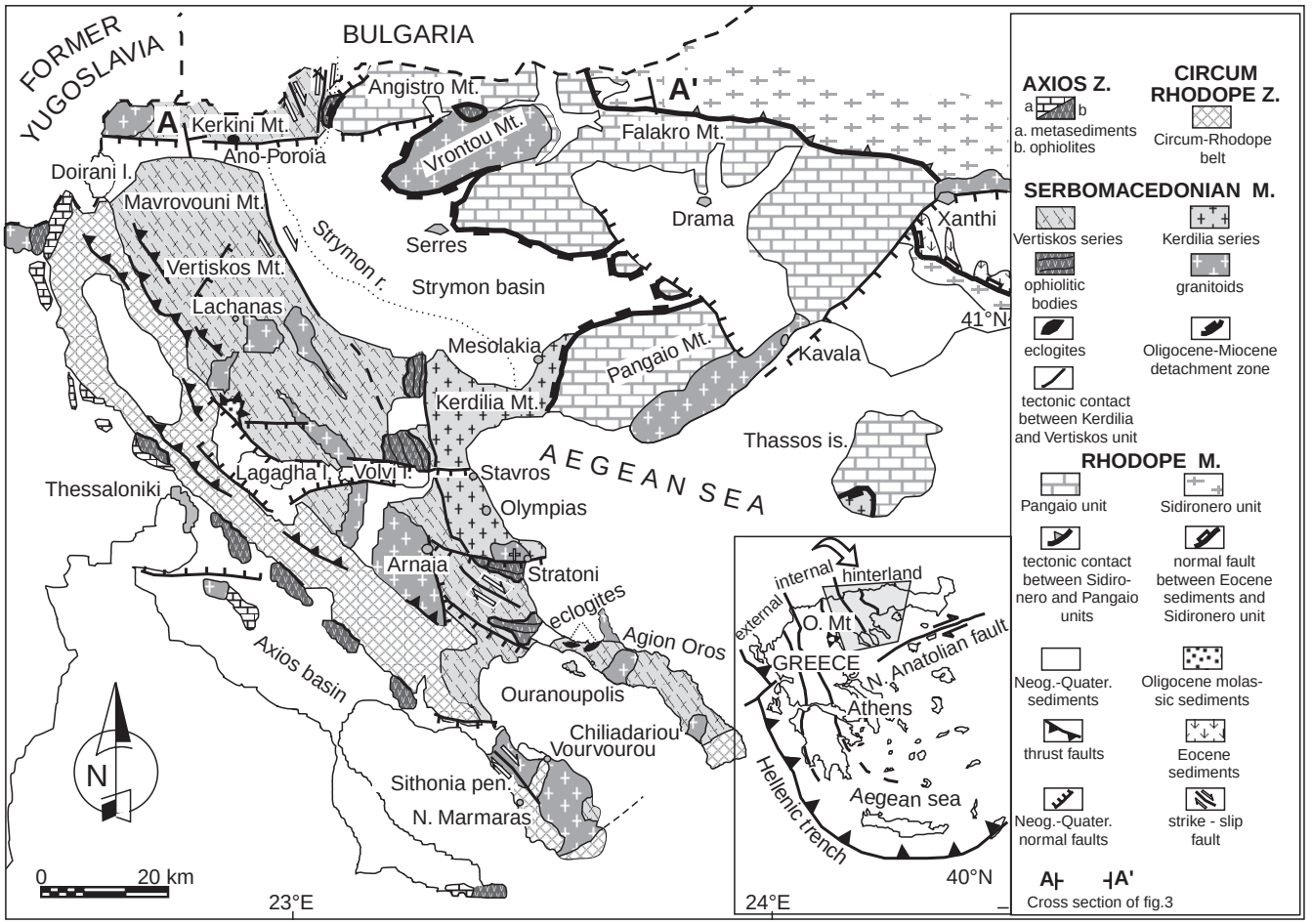

Fig. 1 Simplified map of the Serbomacedonian metamorphic province and its surrounding geological units in northern Greece (based on Kockel et al. 1971; detachment zone traced according to Dinter 1994). The location of the study area is shown in the *inset*

matic and strain analyses. We also discuss the possible relationships of the SRB tectonics to the Rhodope metamorphic complex, proposing a new scheme for the exhumation history of the Hellenic hinterland.

Geological framework

The SRB was divided into two crystalline "series" by Kockel et al. (1971, 1977; Fig. 1): an eastern one, the Kerdilia series, largely composed of migmatitic gneisses, amphibolites and marble, and a western one, the Vertiskos series, composed of intercalations of schists, leucocratic and augen gneisses and amphibolites. From their tectonostratigraphic position the Kerdilia represents the lower unit and the Vertiskos the upper unit.

The tectonometamorphic evolution of the SRB may have started in the Early Palaeozoic or earlier, as proposed by several Yugoslav and Bulgarian workers (Spassov 1961; Bonèev 1966; Dimitrijeviè and Ciriè 1966; Dimitrijeviè 1974). Borsi et al. (1965), Kockel et al. (1977) and Sakellariou (1989) refer to a Late Palaeozoic syntectonic metamorphism under amphibolite facies conditions. During Cretaceous times the SRB was reworked by a syntectonic amphibolite facies metamorphism and later during the Tertiary by a syntectonic retrograde greenschist facies metamorphism (Kockel et al. 1977; Kassoli-Fournaraki 1981; Dixon and Dimitriadis 1984; Chatzidimitriadis et al. 1985; Papadopoulos and Kilias 1985; Sakellariou 1989). Eclogite relics, probably of Mesozoic age, have been found in the Chalkidiki parts of the SRB (Fig. 1; Dimitriadis and Godelitsas 1991; Sidiropoulos 1991). Southwestward low-angle thrusting affecting the SRB rocks is described by Echtler et al. (1987) and Burg et al. (1995).

A remarkable feature is the presence of granitoid bodies that intrude into the SRB (Fig. 1). Borsi et al. (1965) dated pegmatoid bodies as Late Paleozoic intrusions (316–275 Ma Rb–Sr method, whole rock). Further isotopic investigations distinguished granitoids of Jurassic age, such as the granite of Arnea, (155 ± 11 Ma Rb–Sr whole rock; De Wet et al. 1989), and of Cenozoic age, such as the Eocene granites of Sithonia, Ouranoupolis, Chiliandariou (ca. 50 Ma ^{40}Ar–^{39}Ar data, De Wet et al. 1989; Rb–Sr ages, Christofides et al. 1990)

and the Oligocene intrusion of Stratoni (29.6 ± 1.4 Ma K–Ar ages; Papadakis 1971).

The reassessment of the Rhodopian Pangaio/SRB contact as a normal detachment fault (Sokoutis et al. 1993; Dinter and Royden 1993) defines the footwall Rhodopian Pangaio unit as a metamorphic core complex unroofed during the Oligocene–Miocene. The Rhodope massif extends through southern Bulgaria and northeastern Greece, forming a crystalline unit of Palaeozoic or older age (Kronberg et al. 1970; Bonèev 1971; Jones et al. 1992) reactivated during Alpine times (Liati 1986; Ivanov 1988; Kilias and Mountrakis 1990; Burg et al. 1990). The Greek Rhodope has been subdivided by Papanikolaou and Panagopoulos (1981) into an upper tectonic unit (called the Sidironero unit by Kilias and Mountrakis 1990 or the West Thracian gneiss complex by Dinter and Royden 1993; Dinter 1994) and a lower tectonic unit (called the Pangaio unit by Kilias and Mountrakis 1990 or the Rhodope metamorphic core complex by Dinter and Royden 1993). These units are separated by a long NW/SE-trending and NE dipping fault zone, from Xanthi to the Bulgarian border and beyond (Fig. 1), interpreted as a southwestward thrust zone (Papanikolaou and Panagopoulos 1981; Zachos and Dimadis 1983; Kilias and Mountrakis 1990).

Lower-Middle Miocene clastic sediments (Kockel et al. 1977; Psilovikos 1977; Zagorcev 1992) and Oligocene molassic sediments (Kockel et al. 1977) at the base of NW/SE to WNW/ESE-trending basins (Fig. 1) provide the earliest limit for the onset of the normal faults bounding the basins. Furthermore, tectonic basins with Eocene to Oligocene clastic sediments bounded by NW/SE to WNW/ESE-trending high-angle normal faults are developed on the Circum-Rhodope belt (Papadopoulos 1982; Karfakis and Doutsos 1995). Recently, Roussos (1995), using seismic and drilling data, proposed that parts of the Axios basin in the western part of the SRB started to form during Middle Eocene times. In the area south of the town of Xanthi, Eocene sediments consisting of conglomerates and arkose-sandstones with intercalations of nummulitic limestones (Kronberg and Eltgen 1971) also outcrop above the Rhodope metamorphic rocks (Fig. 1).

Deformation pattern

D_{SRB} ductile deformation

The well-preserved fabrics related to the predominant D_{SRB} ductile deformation of the SRB are a penetrative S_{SRB} foliation and the associated stretching lineation, referred to here as L_{SRB} (Fig. 2a). Thus, a lineation–foliation (L–S) fabric is typically formed. The S_{SRB} foliation is mainly NW–SE striking, dipping gently to NE or SW, and is axial planar to isoclinal folds the axes of which are subparallel to the regional stretching lineation. The S_{SRB} fabric is superimposed into a relict S_1 schistosity. Due to transposition, the S_1 foliation is commonly parallel to the main S_{SRB} fabric. The L_{SRB} stretching lineation trends mainly ENE–WSW to WNW–ENE with a gentle plunge (Fig. 2a). L_{SRB} is defined mainly by the dimensional preferred orientation of quartz, feldspar, white mica, biotite, garnet and green amphibole.

The kinematics of D_{SRB} were studied extensively on a regional scale using shear criteria (e.g. Simpson and Schmid 1983; Hanmer and Passchier 1991), in sections parallel to the stretching lineation (X-axis) and perpendicular to the regional foliation (XY-plane). The shear sense indicators show a dominant top-to-ENE to ESE ductile flow (Figs. 2a, 3, 4a). However, a contemporaneous west/southwestward to west/northwestward ductile shear of the tectonic top was also established in places. Determinations of shear sense in the field suggested an approximately threefold predominance of top-to-ENE to ESE sense of shear over top-to-WSW to WNW sense of shear. The contemporaneous activity of both opposite movements is supported by the lack of any overprinting criteria between the two movements and the occurrence of the same critical syn-deformational mineral paragenesis during both movements which record similar pressure–temperature metamorphic conditions. The reason for the opposite movements during D_{SRB} is not clear. The opposite sense of shear could be produced by inhomogeneous strain. Furthermore, the antithetic sense of shear can be attribuded to a coaxial component of deformation during D_{SRB}. Non-spherical rigid object in flows that depart from simple shear can rotate with opposed senses depending on their original orientation (Ghosh and Ramberg 1976). The opposite sense of shear indicated by some feldspar clasts can be related to this kind of effect.

A local coaxial strain during D_{SRB} is also suggested by the occurrence of symmetric structures within the D_{SRB} shear zones, such as symmetric boudins and symmetric elongated clasts, as well as flattened elongated syntectonic mica, quartz and feldspar grains. Moreover, symmetric quartz c-axis fabrics (Fig. 5, Q3, Q4, B1, B2, NP8) in dynamically recrystallized quartz along the S_{SRB} planes reflect a coaxial strain during the final increments of the D_{SRB} deformation and local differences in flow kinematics.

To quantify the degree of non-coaxility (W_m, mean kinematic vorticity number) the graphical approach of Passchier (1987) and Wallis et al. (1993) were used.

In a general shear flow regime, particles with an aspect ratio above a critical value will rotate until they reach a stable orientation, whereas particles below this critical value will rotate without ever finding a stable orientation (Ghosh and Ramberg 1976; Passchier 1987). According to Passchier (1987), the value of this critical aspect ratio, R_c, is a function of the degree of non-coaxiality, W_m, only

$$W_m = (R_c^2 - 1)/(R_c^2 + 1).$$

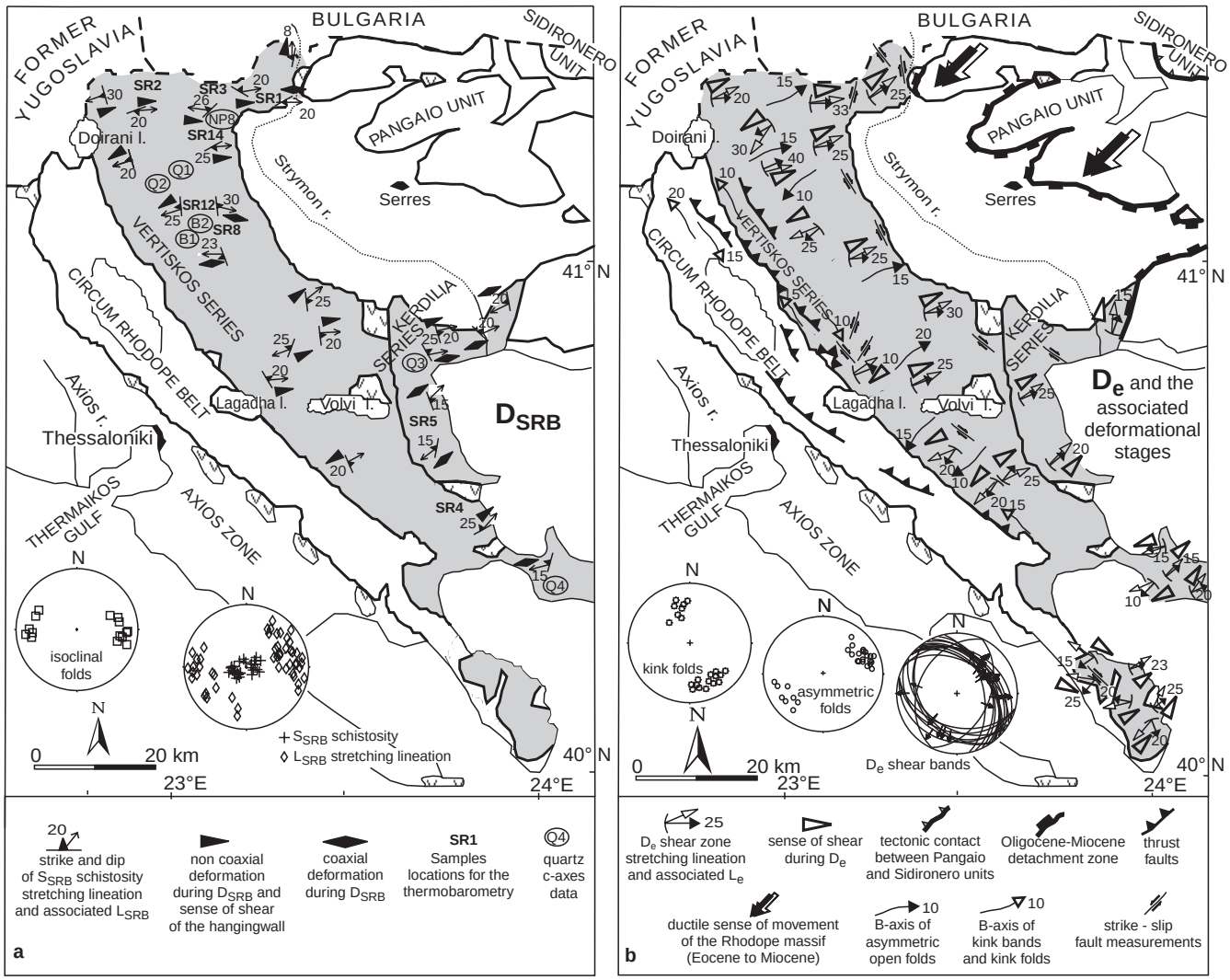

Fig. 2a,b Structural sketch maps of the Serbomacedonian metamorphic province indicating the results of kinematic analysis. **a** The D_{SRB} event. Note the sites of the quartz c-axis measurements (*circles*) of Fig. 5. The samples locations for the geothermobarometric analysis are also shown. **b** The D_e event and the associated deformational stages. Each symbol of shear sense indicator and strike and dip of plane and linear elements represents the mean of 5–20 field measurements in the vicinity of the origin of the symbols. The diagrams are equal-area lower hemisphere projections (Schmidt diagram). For locations see Fig. 1

Samples from the Kerkini Mountains and the Vertiskos Mountains which contain garnet and plagioclase porphyroblasts were analysed by measuring the angle between the long axis of the porphyroblasts and the foliation. The results are shown in Fig. 6. The estimated Wm values are 0.50 for the Kerkini Mountain samples and 0.39 for the Vertiskos Mountains samples. The low degree of non-coaxility emphasizes the importance of the pure shear component in the deformation.

D_e deformation and the relationship between ductile and brittle deformation

Throughout the SRB the D_{SRB} ductile fabric is overprinted by low-angle D_e mylonitic shear zones associated with retrograde greenschist mineral assemblages (Fig. 4b,d,g,h). D_e zones throughout the SRB form a dense network of conjugate shear zones, gently dipping NE or SW (Figs. 2b, 3).

A S_e schistosity associated with a NE/SW-trending L_e stretching lineation characterizes the D_e event. Locally, due to intense transposition during D_e shearing, the S_{SRB} mylonitic fabric is subparallel to the S_e plane. L_e is defined by the strong alignment of syn-D_e greenschist metamorphic minerals along the D_e shear zones. Quartz + chlorite + white mica + plagioclase + epidote ± actinolite is the representative mineral association for the M_e greenschist metamorphism.

Kinematic indicators show both a top-to-NE and antithetic top-to-SW sense of shear, suggesting a strong component of coaxial strain during the D_e event (Figs. 2b, 3, 4g). Asymmetric minor folds with NW/SE-trending fold axes perpendicular to L_e are often devel-

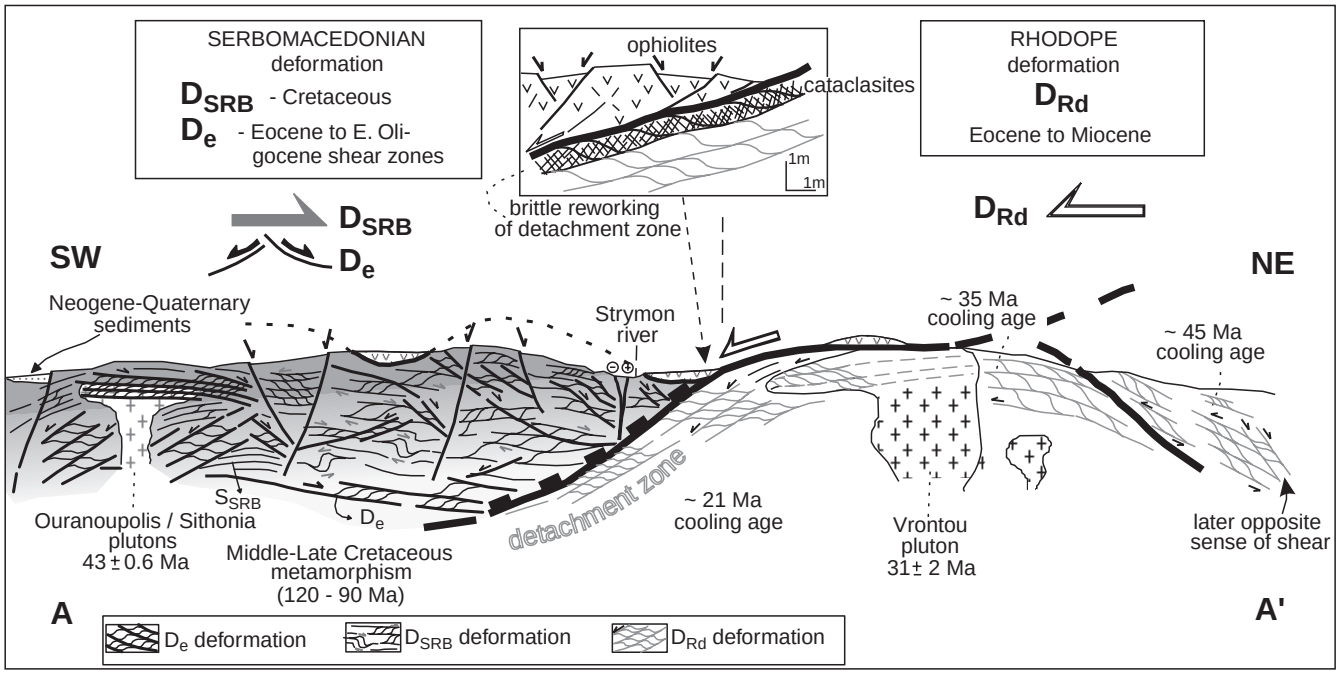

Fig. 3 Schematic cross-section through the Serbomacedonian and western Rhodope metamorphic province in northern Greece, showing the relationships between the two crystalline masses and their dominant studied structures. Cross section not to scale

oped within the D_e shear zones. They are associated with the De Kinematics showing a southwestward or northeastward vergence, when they are related to the SW- or NE-dipping D_e shear zones, respectively.

Asymmetric, open NE/SW-trending folds, subparallel to the L_e stretching lineation (Fig. 2b), deform the greenschist facies M_e mineral assemblage and the S_e schistosity on the micro- to macro-scale. A spaced crenulation cleavage dipping steeply to NW or SE and associated with chlorite and sericite mineralization has been developed axial planar to these folds. The intersection between S_e plane and crenulation cleavage produces a mainly NE/SW-striking intersection lineation that is also subparallel to the L_e mineral elongation lineation. We argue that these folds were formed relatively late in the ductile deformation sequence, under lower P–T metamorphic conditions than the D_e shear zones. We therefore assume that a component of NW/SE-directed subhorizontal shortening accompanied the later stages of the D_e deformation.

Chlorite, sericite-bearing massive cataclasites and pseudo-tachylites are observed in low-angle normal faults, dipping SW or NE, with a mean orientation perpendicular to the L_e stretching lineation (Fig. 4c). Striation on the fault planes trends almost parallel to the L_e stretching lineation. The tectonic contact between the SRB and the underlying Rhodope metamorphic rocks (Fig. 1) is an analogous, SW-dipping low-angle cataclastic shear zone that is defined by Sokoutis et al. (1993), Dinter and Royden (1993) and Dinter (1994), as a normal cataclastic detachment zone along which the SRB was displaced downward to the SW (Fig. 3)

The ductile fabrics of the SRB are overprinted by WNW-ESE- to NW-SE- and NE-SW- to NNE-SSW-striking high-angle, strike-slip faults. Pitches of the striation on the fault surfaces range from 10 to 30°. Kinematic indicators (Hancock 1985) show a general dextral strike-slip displacement for the NW-SE-striking faults and sinistral strike-slip displacement for the NE/SW- to NNE/SSW-trending faults (Figs. 2b, 7a). F rom fault-slip data collected at several localities we computed the palaeostress tensors using the graphical P–T dihedra stress method (Turner 1953) and the grid search method (Gephart and Forsyth 1984). The Appendix describes measurements and determinations made in the field and an outline of the techniques used for stress-tensor calculation. The palaeostress analysis shows that the minimum principal stress axis (σ_3) is approximately subhorizontal in the NE–SW direction, subparallel to the L_e stretching lineation, and the maximum principal stress axis (σ_1) is subhorizontal in the NW–SE direction (Fig. 7a). The computed (σ_3) stress axis orientation indicates that during this younger, more brittle stage of strike-slip faulting, the maximum extension developed in a direction similar to that of the D_e event.

Southwestward-directed younger reverse faults and NW/SE-trending kink bands overprinting the previous ductile fabrics, as well as the high-angle strike-slip fault, are locally developed, mainly in the western SRB and Circum-Rhodope belt (Fig. 2b), suggesting a local development of a NE/SW-trending contractional component. Fault-striae cross-cutting relations, drag

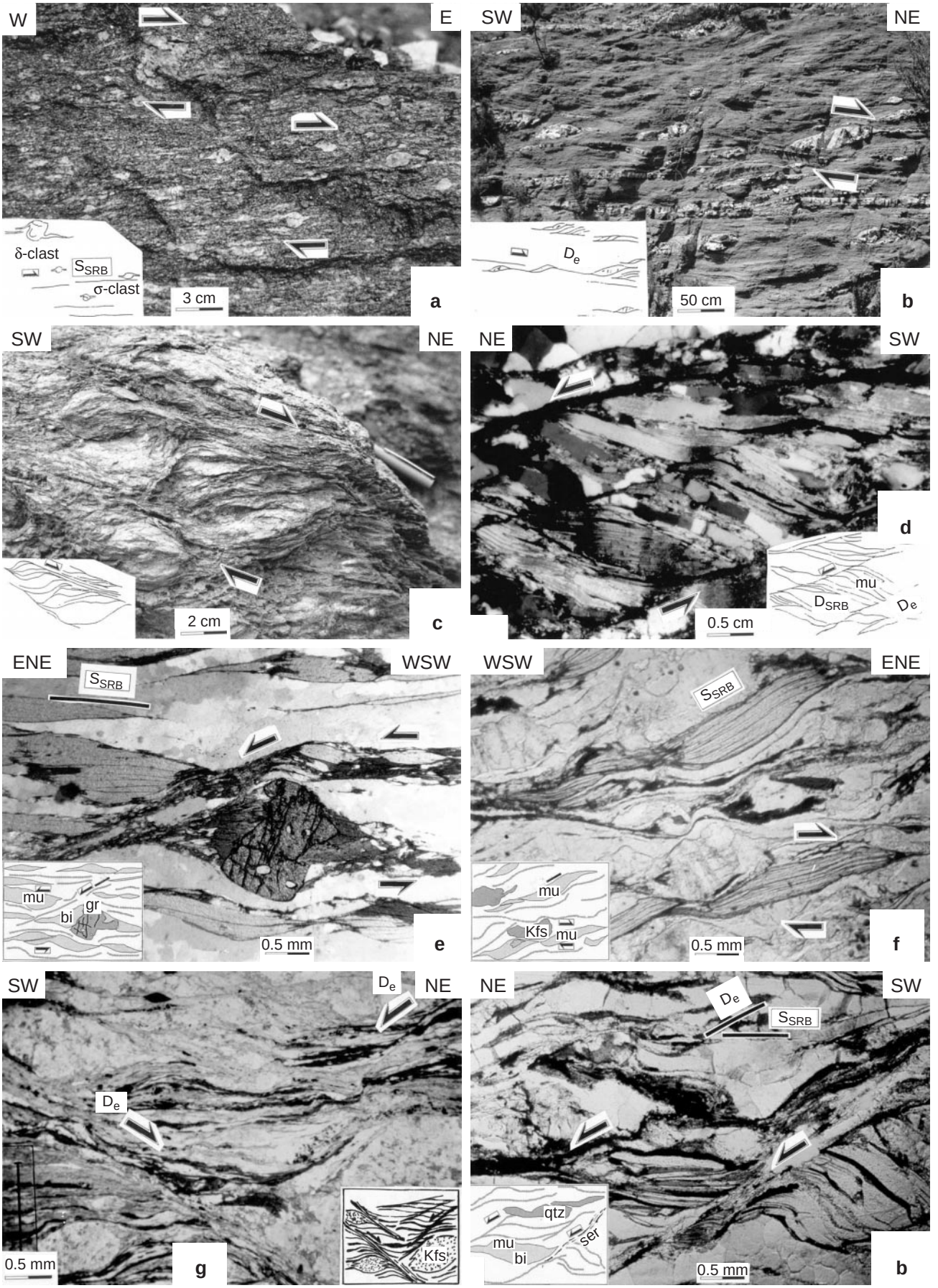
W
E
δ-clast
SSRB
σ-clast
3 cm
a
SW
NE
De
50 cm
b
SW
NE
2 cm
c
NE
SW
mu
DSRB
De
0.5 cm
d
ENE
WSW
SSRB
mu
gr
bi
0.5 mm
e
WSW
ENE
SSRB
mu
Kfs
mu
0.5 mm
f
SW
De
NE
De
0.5 mm
g
Kfs
NE
SW
De
SSRB
qtz
mu
bi
ser
0.5 mm
b

Fig. 4a–h Shear-sense criteria within Serbomacedonian metamorphic rocks related to their deformation. All views are taken in the XZ section. *Black arrows* indicate the sense of shear of the tectonic top. Location names are given in Fig. 1. Mineral abbreviations as in Fig. 8. **a** σ- and δ-type rolling structures within augen gneiss from Mt Kerkini. The sense of shear is top to east. **b** Pervasive shear zones and asymmetric quartzitic boudins within schisto-gneissic rocks of Mt. Kerdilia, Stavros–Olympias road. The sense of shear is top to NE. **c** Low-angle shear bands indicating a down to northeastward movement of the hangingwall, associated with epidote–chlorite mineralization. Schisto-gneissic rocks of Mt. Kerkini. **d** Asymmetric shear bands and mica "fish," from mica-gneisses of Mt. Kerkini (Vertiskos unit). The sense of shear top to NE. **e** Biotite growth in asymmetric pressure shadow of poikiloblastic garnet. White mica and biotite development parallel to the S_{SRB} mylonitic fabric. Top-to-ENE sense of shear is indicated by asymmetric shear band development. Mica-garnet gneisses of Mt. Mavrovouni. **f** Muscovite along the S_{SRB} plane. Shear band asymmetry shows a top-to-ENE sense of shear. Mica gneisses northern of Lagadha lake. **g** Conjugate set of shear bands with opposite top-to-NE and SW sense of shear. Mica gneisses at the Arnaia area. **h** Shear bands associated with white mica, chlorite, epidote mineralization. Top-to-NE sense of shear. Mica-gneisses of Mt.Vertiskos, Lachanas-Serres road. *bi* biotite; *mu* muscovite; *ser* sericite; *kfs* K-feldspar; *qtz* quartz; *gr* garnet

and kink folds formation as well as mineral retrogressions along the fault zones were used as overprinting criteria.

High-angle conjugate, normal faults cross-cutting all previous structures and representing the final stages of the deformation form a dense network of fractures. Striations pitches on their fault planes range from 75 to 85°. Figure 1 illustrates the main faults of this fracture network. Psilovikos (1977) and Pavlides and Kilias (1987), based on the fault geometry and kinematics, fault-striae cross-cutting relationships, morphotectonic data and the stratigraphy of the Neogene basins on the SRB, interpret the NW/SE-trending faults as the older structures of this SRB fracturing. These are associated with a NE/SW-trending, almost dip-slip striation on their planes. Palaeostress analysis using both the P–T dihedra stress method and grid search method (see Appendix) reveals that the minimum stress axis (σ_3) is almost horizontal in the NE–SW direction sub-parallel to L_e, whereas the maximum stress axis (σ_1) is almost vertical (Fig. 7b). Thus, we can assume that at least during the onset of the high-angle normal faulting in the SRB the maximum extension developed in accordance with that during the D_e, as well as during the high-angle strike-slip faulting.

Relation between deformation and metamorphism

The metamorphic P–T conditions were derived from mineral compositions and textural equilibria. Mineral assemblages with synkinematic growth with respect to the D_{SRB} event were used for this purpose. The S_{SRB} fabric in metapelitic rocks is composed mainly of planar biotite and white mica (Fig. 4e,f). Biotite and white

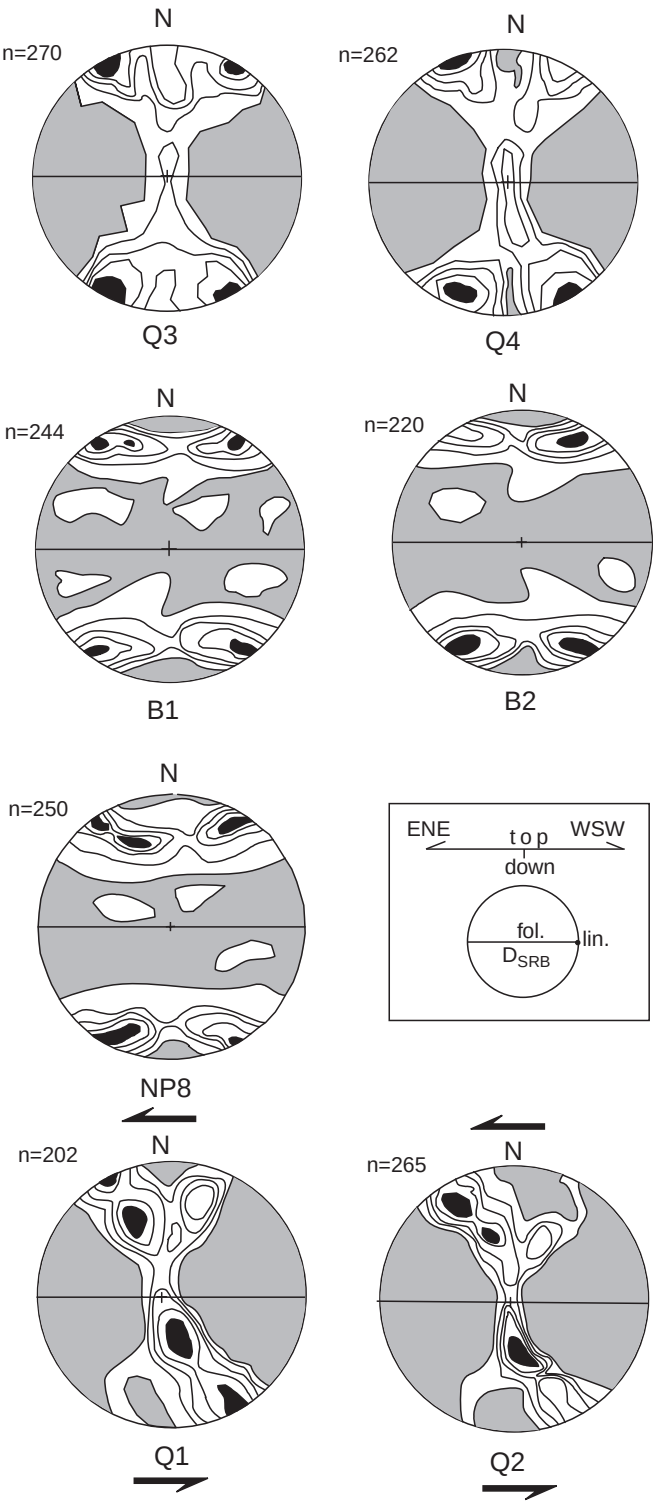

Fig. 5 Representative Quartz c-axis fabrics from synkinematic to the D_{SRB} recrystallized quartz grains in gneissic rocks from the Vertiskos unit. Lower hemisphere, equal-area projections. The foliation–lineation refers to the D_{SRB} fabric; *n* number of measurements; contour interval = 1; uniform density. Locations are given in Fig. 2a

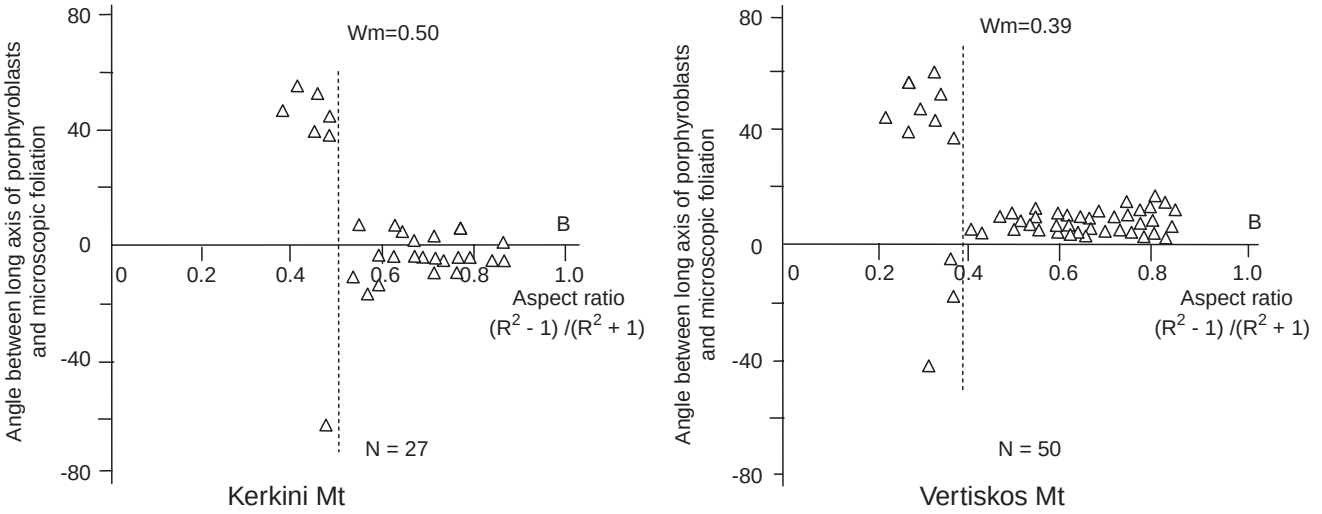

Fig. 6 Porphyroblasts analysis to quantify the degree of non-coaxiality according to Passchier (1987) method. Values of Wm: 0.50 and 0.39

mica are also found in pressure shadows at the margins of garnets, parallel to the S_{SRB} fabric (Fig. 4e). In amphibolites S_{SRB} is defined mainly by green amphibole. Syn-D_{SRB} development of minerals is indicated by their strong alignment parallel to the S_{SRB} foliation and L_{SRB} lineation (Fig. 4e,f), by sigmoidal forms of the S_i internal schistosity in rotated oligoclastic plagioclase or garnet, and its continuity in agreement with the matrix foliation $S_e = S_{SRB}$, as well as by the dynamic recrystallization of quartz along the S_{SRB} planes. Syn-deformational growth of garnet blasts is deduced from the mylonitic external foliation deflecting around the blasts at an early stage of growth and being eventually overgrown and preserved within the blasts. D_{SRB} was locally followed by a static postkinematic annealing indicated by polygonal quartz microfabrics with equilibrated grain boundaries and triple points.

The critical syn-D_{SRB} mineral paragenesis in metapelitic rocks is quartz + white mica + biotite + garnet + oligoclase ± staurolite ± kyanite. In amphibolites the critical syn-D_{SRB} mineral assemblage is tschermakitic hornblende + oligoclase + epidote + biotite + quartz ± garnet ± white mica.

Microprobe analyses were carried out in minerals defining the syn-D_{SRB} paragenesis. Sample locations are shown in Fig. 2a. Mineral chemistries of representative phases are given in Table 1. The P–T conditions for the syn-D_{SRB} metamorphism were estimated on the basis of garnet–biotite (Ferry and Spear 1978), muscovite–biotite (Hoisch 1989) and garnet–muscovite (Hynes and Forest 1988) geothermometers, the hornblende–plagioclase geothermobarometer (Plyusnina 1982), the phengite component geobarometer (Massonne and Schreyer 1987) and the garnet–amphibole–plagioclase (Kohn and Spear 1989) geobarometer, as well as using amphibole and biotite compositions (Laird et al. 1984; Schreurs 1985). The PTOXY computer software (Nasir 1994), was used to facilitate the temperature and pressure calculations. The P–T metamorphic conditions were estimated at 4.5–7.5 kbar and 510°–580 °C, respectively (Figs. 8, 9). The equilibrium temperatures are also supported by the anorthite content of the plagioclases (An_{17-25}). Similar P–T metamorphic conditions were deduced using the Ti (Ti = 0.069–0.156) and Al6 (Al6 = 0.315–0.533) contents in biotite (Schreurs 1985), pointing to a low- to medium-grade amphibolite facies. Amphibole compositions plot in the common field of low and medium pressures and close to the oligoclase isograd in the diagram of Laird et al. (1984; Fig. 9b). It is noted that due to uncertainties concerning the thermodynamic constants involved, the P–T estimates resulting from different geothermo- and barometric calibrations carry a minimum error of ±50 °C and ±1 kbar (Spear and Rumble 1986).

The systematically decreasing phengite component, from approximately $Si^{4+} = 3.18$ atoms p.f.u (per formula unit) in the core to $Si^{4+} = 3.10$ atoms p.f.u. in the rim of the syn-D_{SRB} white micas, is ascribed to a path with decreasing P/T quotient. The derived pressure values range from approximately 5.0 kbar in the cores to approximately 3.0 kbar in the rims of white mica crystals. The change in chemical composition from the core to the rim of synkinematic garnets reflects a change in temperature conditions during their evolution (Spear et al. 1990). The component of three independent parameters [spessartine, grossular content and Fe/(Fe + Mg) ratio] in the core and the rim of syn-D_{SRB} garnets suggest decreasing temperatures during their

Fig. 7a,b Paleostress analysis and geometry of fault-slip kinematics using the P–T and grid search methods. Lower hemisphere, equal-area stereographic projections. The fault planes and slip direction are shown. Data from: **a** high-angle dextral and sinistral strike-slip faults; and **b** high-angle normal faults. $\sigma_1 > \sigma_2 > \sigma_3$ (P>B>T) the principal axes for stress ellipsoid

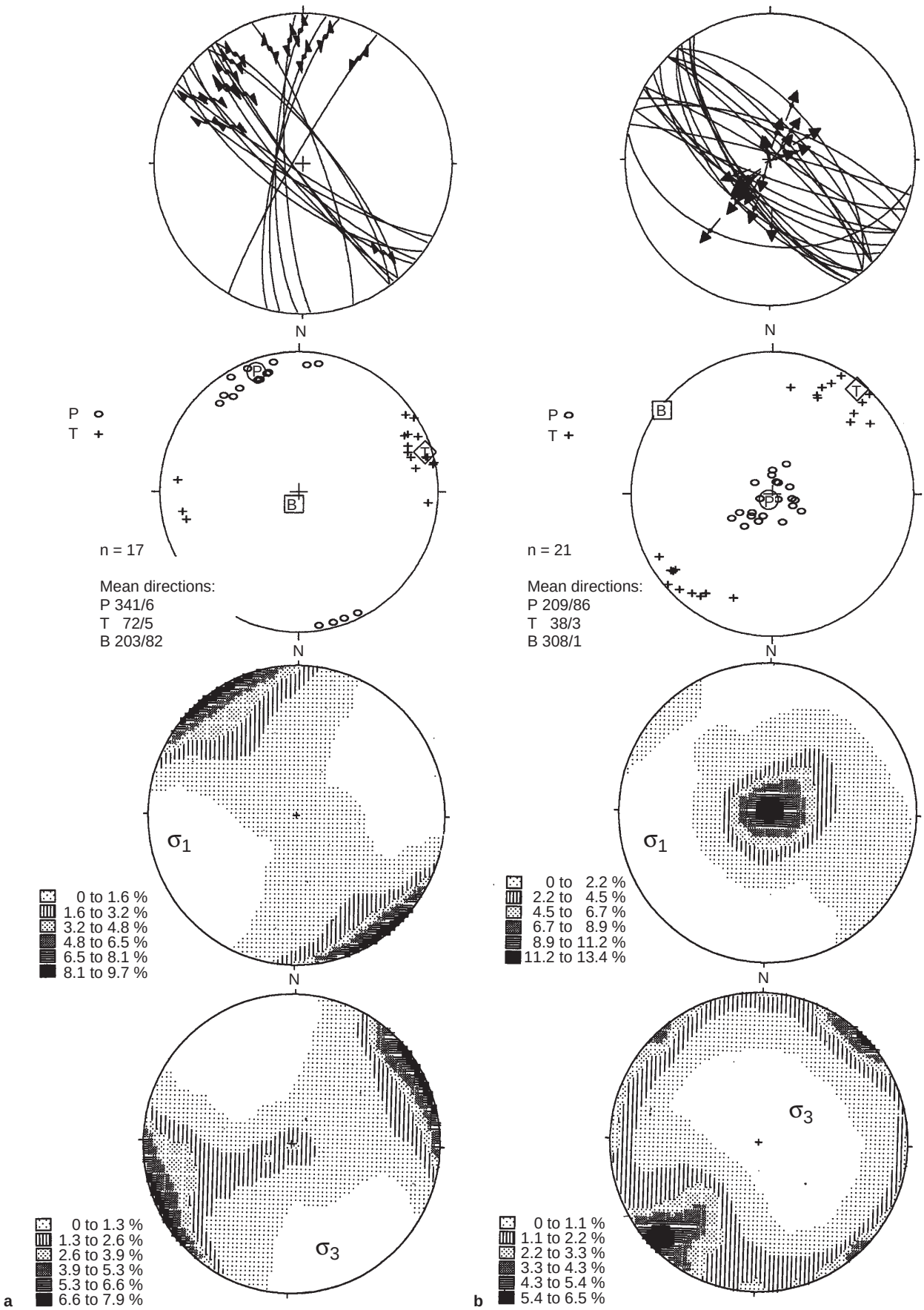
N
P
T
B
n = 17
Mean directions:
P 341/6
T 72/5
B 203/82
σ1
0 to 1.6 %
1.6 to 3.2 %
3.2 to 4.8 %
4.8 to 6.5 %
6.5 to 8.1 %
8.1 to 9.7 %
σ3
0 to 1.3 %
1.3 to 2.6 %
2.6 to 3.9 %
3.9 to 5.3 %
5.3 to 6.6 %
6.6 to 7.9 %
a
n = 21
Mean directions:
P 209/86
T 38/3
B 308/1
0 to 2.2 %
2.2 to 4.5 %
4.5 to 6.7 %
6.7 to 8.9 %
8.9 to 11.2 %
11.2 to 13.4 %
0 to 1.1 %
1.1 to 2.2 %
2.2 to 3.3 %
3.3 to 4.3 %
4.3 to 5.4 %
5.4 to 6.5 %
b

Table 1 Representative microprobe analyses of syn-D_{SRb} growth minerals. *SR3* garnet, mica schist; *SR2* garnet, two mica gneisses; *SR14* amphibolite; *R* rim; *C* core

Oxide	Garnet			Muscovite		Biotite		Plagioclase		Amphibole
	SR3	SR2		SR3		SR2	SR3	SR2	SR14	SR14
	GR2R	GR3C	GR3R	MO4C	MO4R	BI3	BI4	PLG5	PLG3	AMP4
SiO_2	38.48	38.75	38.59	48.80	47.87	37.30	35.90	60.53	61.78	42.84
TiO_2	0.00	0.05	0.000	0.80	0.72	2.14	1.65	0.00	0.00	0.63
Al_2O_3	21.45	21.60	21.62	33.34	34.57	17.76	20.12	24.57	23.22	13.31
Cr_2O_3	0.05	0.000	0.05	–	–	–	–	–	–	0.00
FeO	33.20	26.85	26.86	1.17	1.19	17.44	19.87	0.00	0.12	16.15
MnO	3.49	2.76	1.19	0.26	0.00	0.06	0.06	–	–	0.21
MgO	1.91	2.73	2.23	0.77	0.55	11.32	8.27	0.00	0.00	9.54
CaO	1.37	7.35	9.23	0.00	0.00	0.00	0.00	5.66	4.76	10.92
Na_2O	–	–	–	1.17	1.48	0.63	0.48	9.47	10.11	1.86
K_2O	–	–	–	8.96	8.83	8.81	8.38	0.06	0.15	1.62
Total	99.93	100.10	99.78	95.28	95.20	95.46	94.73	100.30	100.14	97.08
Formulae on the basis of 23O		12 O			11O		11 O		8 O	
Atoms										
Si	3.079	3.049	3.043	3.215	3.157	2.792	2.730	2.963	2.750	6.417
Al^4	0.000	0.000	0.000	0.785	0.843	1.208	1.270	1.289	1.218	1.583
Al^6	2.023	2.003	2.010	1.804	1.843	0.359	0.533			0.687
Fe^{3+}	0.000	0.000	0.000							0.303
Fe^{2+}	2.222	1.767	1.772	0.064	00.066	1.092	01.264	00.000	00.004	1.679
Ti	0.000	0.003	0.000	0.040	0.036	0.120	0.094	0.000	0.000	0.091
Cr	0.003	0.000	0.003	–	–	–	–	–	–	0.000
Mn	0.237	0.184	0.080	0.015	0.000	0.004	0.004	–	–	0.032
Mg	0.227	0.321	0.263	0.076	0.054	1.264	0.937	0.000	0.000	2.207
Ca	0.117	0.620	0.780	0.000	0.000	0.000	0.000	0.270	0.227	1.740
Na	–	–	–	0.149	0.189	0.091	0.071	0.817	0.873	0.260 (M4)
										0.363 (A)
K	–	–	–	0.753	0.743	0.842	0.813	0.003	0.009	0.309
X_{Mg}	0.093	0.154	0.129	0.541	0.451	0.537	0.426	–	–	0.568
Sps	0.084	0.064	0.028							
Grs	0.040	0.213	0.268							
Fe/(Fe + Mg)	0.907	0.846	0.871							

evolution: The grossular content and Fe/(Fe + Mg) ratio increase from 0.162 to 0.268 and 0.846 to 0.871, respectively, whereas the spessartine content decreases from 0.046 to 0.021.

The syn-S_{SRB} amphibolite facies mineral assemblages suffered during D_e a retrogressive greenschist overprint. Replacement of biotite by chlorite and garnet by sericite and chlorite in metapelitic rocks, as well as replacement of tschermakitic amphibole by actinolite and chlorite in the amphibolites, is observed. Replacement of the syn-D_{SRB} minerals took place along their cleavage planes or within microfracture zones and pull-apart offsets, as well as in pressure shadows. Chlorite, actinolite and white mica retrogression assemblages strike generally NE–SW, parallel to L_e. Synkinematic overgrowth and recrystallization of chlorite, actinolite and white mica, as well as dynamic recrystallization of quartz, has continued along the low-angle D_e shear zones (Fig. 4h) forming the L_e stretching lineation.

Age of deformation

To determine the age of deformation it is of special interest to consider the age and tectonic position of the Sithonia, Ouranoupolis and Stratoni granitoid bodies (Figs. 1, 3).

The syntectonic character of both the Eocene Sithonia and Ouranoupolis granitoids with respect to the regional deformational state of the surrounding metamorphic rocks is described in detail by Sapountzis et al. (1976), De Wet et al. (1989), D'Amico et al. (1991) and Tranos et al. (1993). This deformation in the Sithonia area is defined by Tranos et al. (1993) as a mainly northeastward low-grade metamorphic facies shearing accompanied during its later stages by a NW/SE-directed component of shortening. We recognized this deformation in the whole SRB domain and ascribe its associated structures to the D_e event (Figs. 2b, 4, 10b).

In contrast, the Mid-Oligocene Stratoni granitoid appears as a posttectonic, unaffected by ductile deformation body cutting across the dominant regional

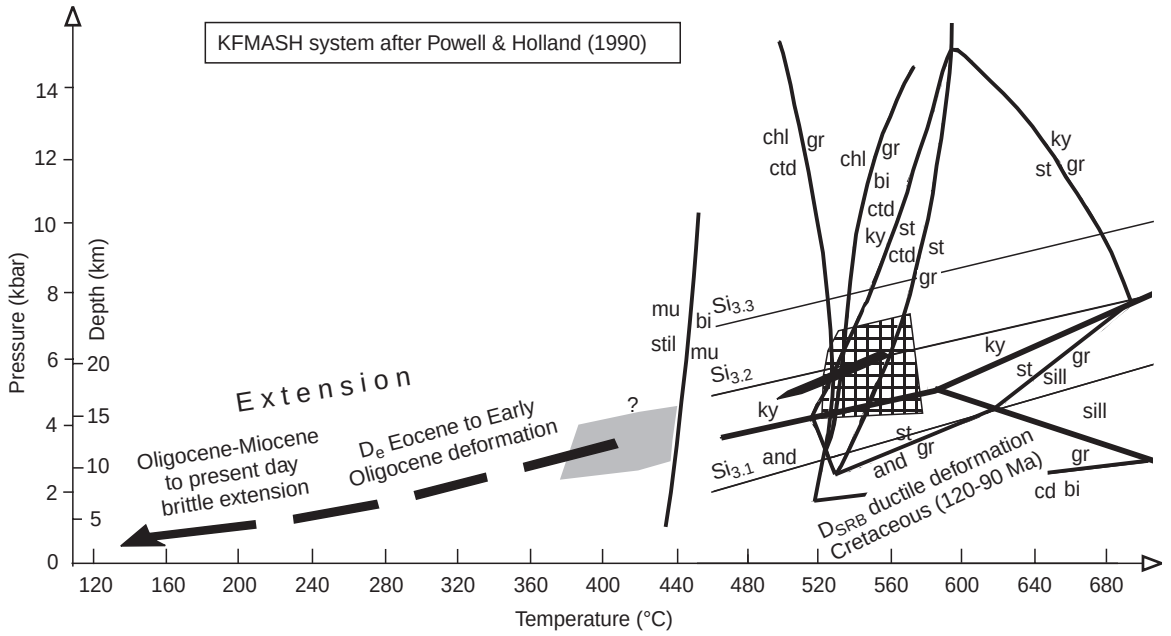

Fig. 8 Pressure–temperature–time deformation relationship of the Serbomacedonian metamorphic rocks from the Cretaceous to the Neogene. The relevant equilibria involved in the stability field of the syn-D_{SRB} and syn-D_e mineral assemblages are shown. Note stability curves for $Si_{3.1–3.3}$ phengite according to Massone and Schreyer (1987). The *hatched area* is the P–T domain estimated by geothermobarometry for the D_{SRB} event; *dotted area* corresponds to the peak of the syn-D_{Sbe} metamorphism. *ky* kyanite; *gr* garnet; *st* staurolite; *and* andalusite; *sill* sillimanite; *bi* biotite; *mu* muscovite; *chl* chlorite; *stil* stilpnomelane; *ctd* chloritoid; *cd* cordierite; *ser* sericite; *kfs* K-feldspar

fabric of the surrounding SRB metamorphic rocks (Papadakis 1971). Consequently, an Early Oligocene minimum age for the ductile deformation of the SRB can be considered.

The metamorphic peak of the syn-metamorphic D_{SRB} deformation has been reached before emplacement of the Sithonia and Ouranoupolis granitoids. Using K–Ar and Rb–Sr mineral ages of white mica, biotite and hornblende, Papadopoulos and Kilias (1985) dated the main syn-metamorphic fabric of the SRB as Middle to Late Cretaceous (120–90 Ma). Dixon and Dimitriadis (1984) also describe a Mid- to Late Cretaceous deformational event that has affected the SRB. Older tectonic events (Borsi et al. 1965; Papadopoulos and Kilias 1985; and Sakellariou 1989) may have affected the SRB but were strongly overprinted by the Cretaceous deformation.

The greenschist facies D_e deformational event which is imprinted on the Eocene Sithonia and Ouranoupolis granitoids, but which has not affected the Mid-Oligocene Stratoni granite, should have developed at least during Eocene times and until the Early Oligocene. The NW–SE shortening component which accompanied the later stages of the D_e event should have started to act during the Late Eocene–Early Oligocene. The high-angle normal faulting developed during the Miocene–Pliocene (Kockel et al. 1977; Psilovikos 1977; Zagorcev 1992). Therefore, the chlorite–sericite bearing low-angle normal faults, possibly associated with the Oligocene molasse sediments that are described by Kockel et al. (1977), the conjugate set of the strike-slip faults, and the younger southwestward thrusting at the western SRB parts and the Circum–Rhodope belt, must have been developed during Oligocene to Miocene times. The SW-vergent thrusting should have been developed during Late Oligocene–Early Miocene since the molasse sediments are overthrusted by the SRB metamorphic rocks in southwestward direction (Figs. 1, 2b).

Tectonic setting

D_{SRB} deformation

The D_{SRB} ductile structures give no clear evidence for the tectonic significance of the D_{SRB} mylonitic shear zones, because stretching lineation parallel to isoclinal folds, asymmetric structures and mylonitic fabric may develop in either a contractional or an extensional regime; however, decreasing pressure and temperature conditions were recognized during D_{SRB} development. This is indicated by the change in chemical composition from the core to the rim of the syn-D_{SRB} white mica and garnet. On the other hand, several points (indicated below) provide evidence for large-scale subhorizontal crustal stretching during the Cretaceous syn-metamorphic D_{SRB} event. Many of these have already been used by other authors as indicators for an extensional tectonic regime for other areas, e.g. the Alps, Mexico and the Cyclades (e.g. Ratschbacher et al. 1989, 1991; Lee and Lister 1992):

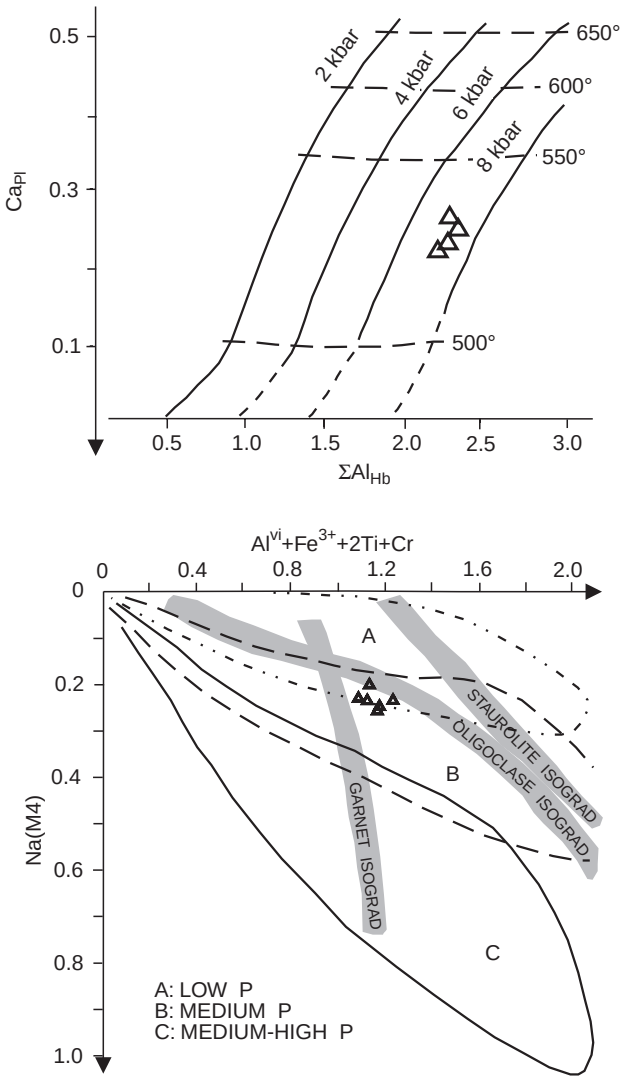

Fig. 9 **a** Hornblende – plagioclase geothermobarometer (Plyusnina 1982). **b** Plot of amphibole microprobe analyses in the diagram by Laird et al. (1984)

1. An important component of coaxial ENE/WSW- to WNW/ESE-directed extension, subparallel to the shallowly dipping S_{SRB}, leads to subvertical thinning and subhorizontal stretching.
2. Burg et al. (1990) mentioned for the uppermost Rhodopian domain of the Asenica unit in northern Bulgarian area an ENE-vergent, flat-lying shear deformation related to Late Cretaceous amphibolite facies metamorphism. This comprises a kinematic regime that coincides with the one described here for the SRB. This east/northeastward ductile shearing of the upper Rhodopian unit is possibly associated with crustal extension and exhumation (Burg et al. 1990). The Asenica unit (Burg et al. 1990) comprises a sequence of metamorphic rocks similar to the SRB and may form a remnant of the SRB on top of the Rhodope units. Therefore, the D_{SRB} deformation must be related to the same extensional tectonic regime that has been mentioned for the Asenica unit during the Cretaceous.
3. Basins of Late Cretaceous age on the uppermost Rhodopian domain (as the Asenica unit) are associated with a subhorizontal, brittle extensional component of deformation as described by Nachev (1993) for central and northern Bulgaria. These Cretaceous basins formed simultaneously with the high-temperature D_{SRB} event in the footwall.

Following Sengör et al.'s (1984) view on the Cimmerian orogenesis, both the SRB and the Rhodope may have been part of a single continental block during the Cretaceous. The D_{SRB} deformation seems to be related to the Cretaceous continent–continent collision between the Rhodopian (SRB included) and Moesian fragments described by Burchfiel (1980), Bonèev (1988), Dercourt et al. (1993) and Ricou (1994). North- to northeastward thrusting in the northern parts of the Rhodopian fragment is associated with this continental collision. Following our description about the structural features of the D_{SRB} event, D_{SRB} could have been developed in an inner area behind the frontal thrust belt and contemporaneous with it, associated with subhorizontal crustal stretching and unroofing. Furthermore, southwestward syn-metamorphic thrusting of the lower Rhodopian units during the Cretaceous (Burg et al. 1990, 1996) may have taken place simultaneously with the D_{SRB} ductile extensional event in the middle SRB crustal levels (Fig. 10a).

D_e deformation and the associated deformational stages

Several lines of evidence favour a subhorizontal bulk extension during the D_e event:

1. Eocene basin formation in the hangingwall of the Circum-Rhodope belt rocks is associated with subhorizontal NE/SW-directed brittle extension (Fig. 10b; Karfakis and Doutsos 1995). Simultaneously, D_e deformation under greenschist facies conditions took place at deeper structural levels in the SRB. Therefore, a kinematic link between the ductile D_e shear zones and normal faulting in the

Fig. 10a–e Schematic crustal-scale transects showing the kinematics and structural evolution of the Serbomacedonian/Rhodope metamorphic province from the Cretaceous onwards. **a** Continent-to-continent collision during the Cretaceous between the Moesian and Rhodope (including Serbomacedonian) fragments and development of D_{SRB} deformation. **b–e** The successive deformational stages from the Eocene to the present-day position of the Serbomacedonian/Rhodope metamorphic province that characterize its progressive uplift history, due to large-scale subhorizontal continental stretching. *PG* Rhodope Pangaio unit; *SD* Rhodope Sidironero unit; *CRB* Circum Rhodope Belt; *OPH* ophiolites

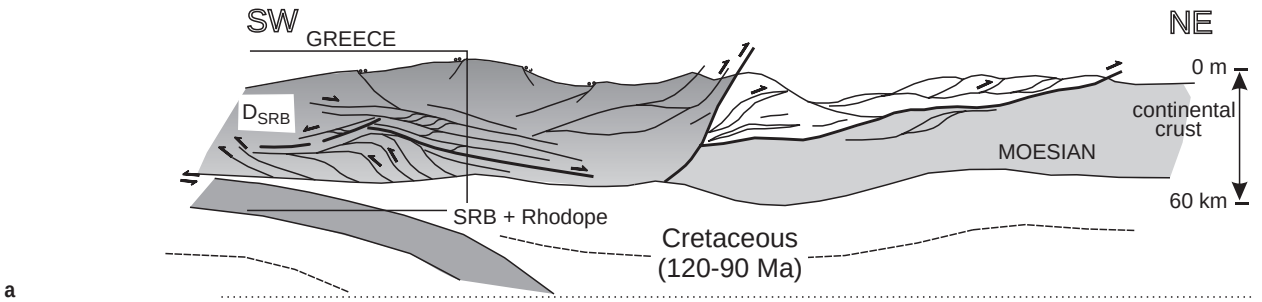
SW
GREECE
NE
0 m
D_{SRB}
continental crust
MOESIAN
60 km
SRB + Rhodope
Cretaceous
(120-90 Ma)

a

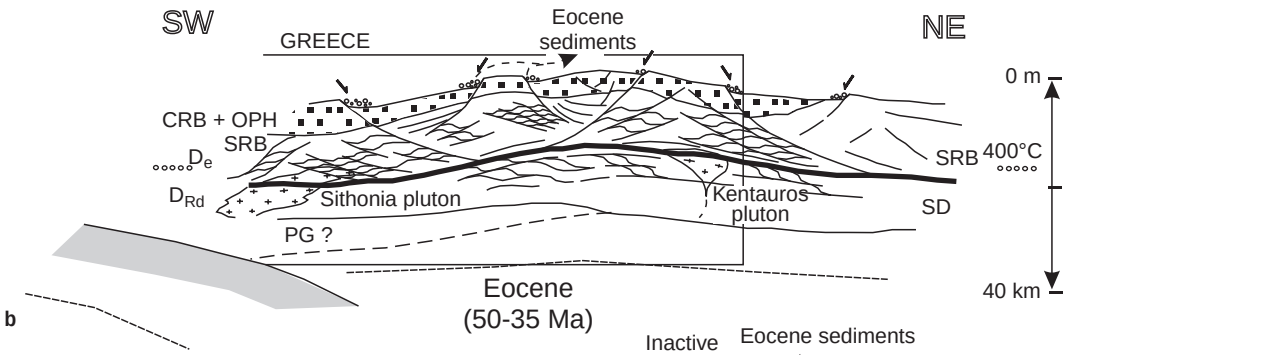
SW
GREECE
Eocene sediments
NE
0 m
CRB + OPH
SRB
D_e
D_{Rd}
Sithonia pluton
Kentauros pluton
PG ?
SRB
400°C
SD
40 km
Eocene
(50-35 Ma)

b

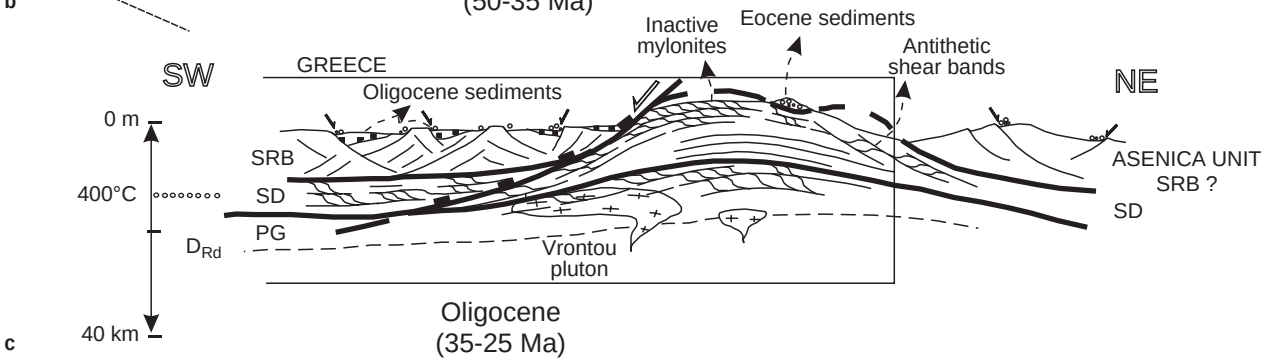
Inactive mylonites
Eocene sediments
Antithetic shear bands
SW
GREECE
Oligocene sediments
NE
0 m
SRB
400°C
SD
PG
D_{Rd}
Vrontou pluton
ASENICA UNIT
SRB ?
SD
40 km
Oligocene
(35-25 Ma)

c

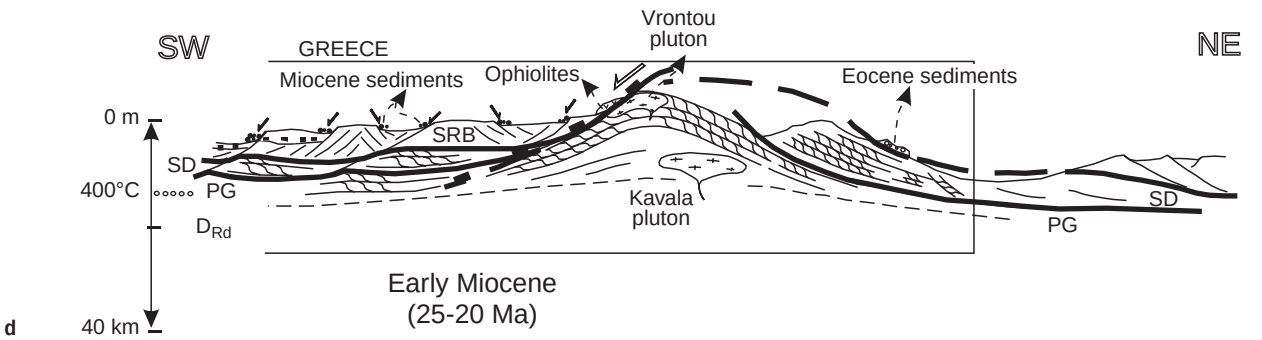
Vrontou pluton
SW
GREECE
NE
Miocene sediments
Ophiolites
Eocene sediments
0 m
SRB
SD
400°C
PG
D_{Rd}
Kavala pluton
SD
PG
40 km
Early Miocene
(25-20 Ma)

d

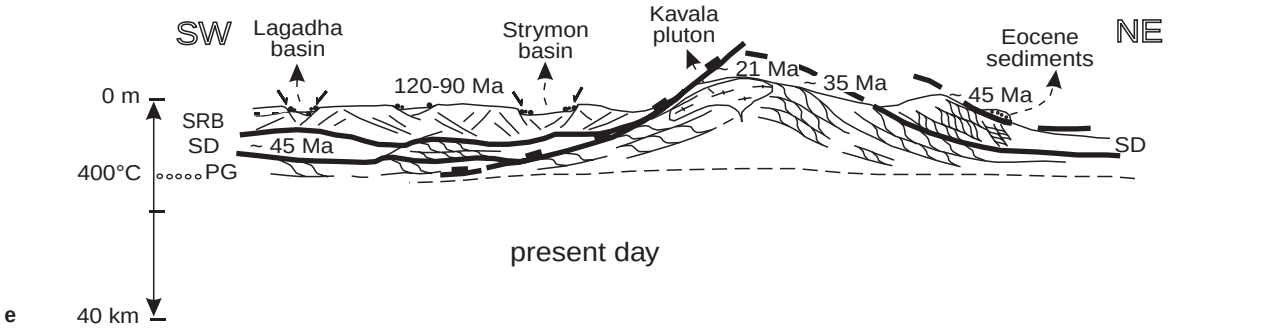
SW
Lagadha basin
Strymon basin
Kavala pluton
NE
Eocene sediments
120-90 Ma
21 Ma
35 Ma
45 Ma
0 m
SRB
SD
~ 45 Ma
400°C
PG
SD
40 km
present day

e

upper crust is deduced. In addition, the deeper crustal parts of the upper Rhodope Sidironero unit are syntectonically metamorphosed during the Eocene under amphibolite facies conditions ($P \sim 7$–9 kbar, $T \sim 550$–$650\,^{\circ}C$; Liati 1986; Mposkos et al. 1990; Kilias and Mountrakis 1990). The Sidironero unit is also exposed south of Xanthi beneath a NE-dipping low-angle fault directly and overlain by Eocene sediments (Figs. 1, 10c). This implies tectonic denudation and exhumation of the Sidironero unit. Duplication is nowhere observed. Therefore, the low-angle fault separating the unmetamorphosed Eocene sediments from the mylonitic rocks can be explained as a low-angle normal detachment fault, which evolved from an upper crustal level normal fault zone into ductile shears of Eocene age at depth (Fig. 10c). According to the model of Wernicke (1981) and that of Lister and Davis (1989), downward translation along this fault juxtaposed the unroofed, mid-crustal footwall Sidironero mylonitic rocks with shallow crustal rocks, resulting in tectonostratigraphic omission.

2. An important component of coaxial subhorizontal NE/SW-trending extension is suggested by the conjugate D_e shear zones that are associated with downward sense of movement, either to the NE or SW (Fig. 10c).
3. Transition from the ductile Eocene D_e deformation to the brittle deformation from the Oligocene onward with similar NE/SW-oriented maximum extension indicates that the SRB has undergone unroofing toward the surface, at least since the Eocene.
4. The uppermost ophiolitic remnants of the Tethys ocean directly overlie the SRB metamorphic rocks, by omission of all the slightly metamorphosed Circum-Rhodope belt rocks (Fig. 3).

It is possible that the D_e deformational regime developed simultaneously with the Eocene high-pressure/low-temperature compressional event that created the blueschist belt, outcropping today in the Olympos–Ossa area (Godfriaux 1968; Schermer et al. 1989; Kilias et al. 1991), Euboia area (Katsikatsos 1977) and Cyclades area (Dürr et al. 1978; Andriessen et al. 1979; Alther et al. 1979; Blake et al. 1981; Schliestedt et al. 1987; Gautier et al. 1993). Thus, during the Eocene, nappe stacking and crustal thickening occurred in the accretionary wedge of the subduction zone while crustal thinning associated with thermal overprint and

Fig. 11 The Tertiary tectonic setting of the Serbomacedonian massif. Not to scale

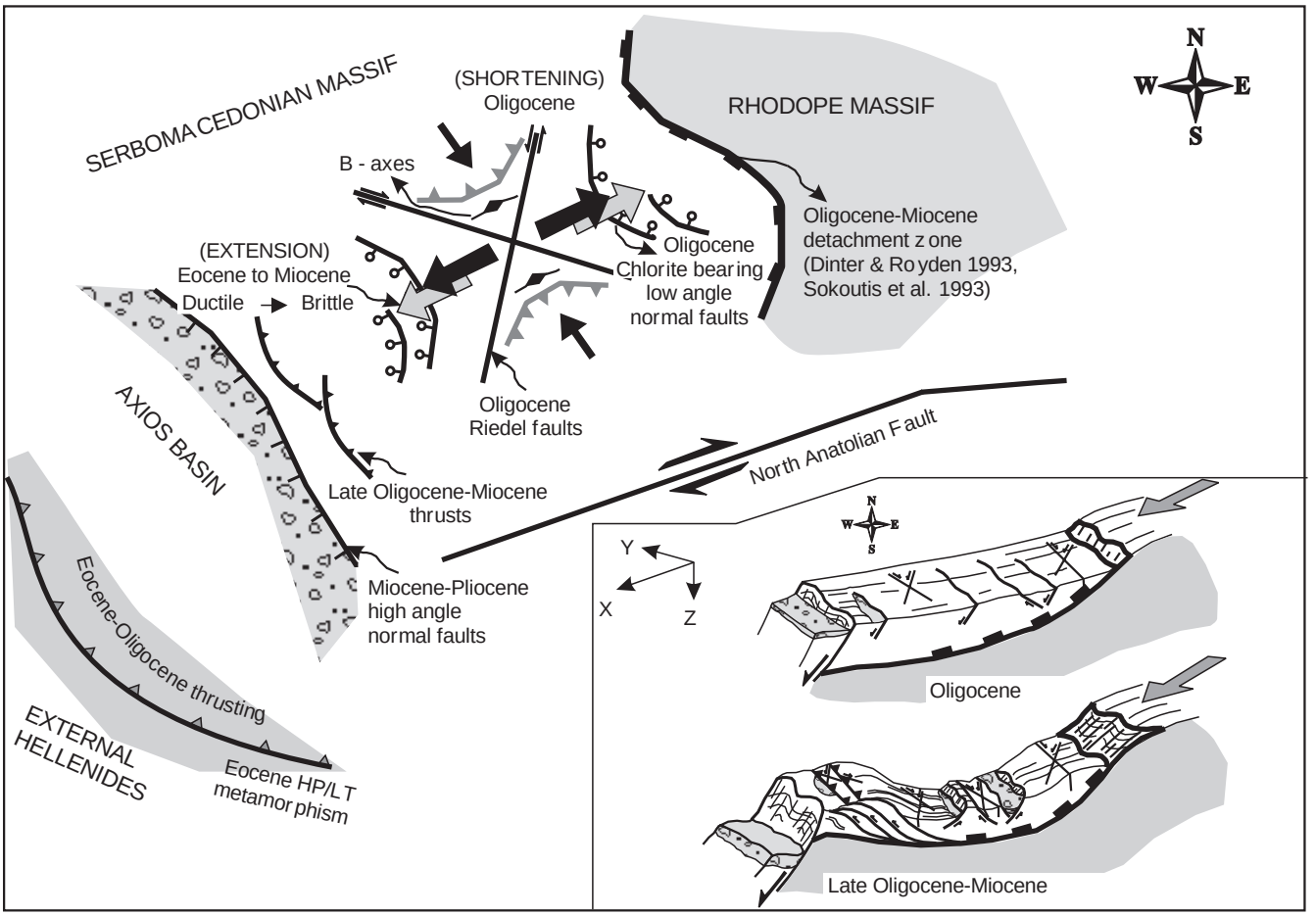

collapse developed in the inner SRB and Rhodope areas (Figs. 10b, 11). Northeast/southwest SRB crustal extension continued under more brittle conditions during Oligocene–Miocene as is suggested by the low-angle normal faults and the SRB normal detachment.

The NE–SW shortening structures that accompanied the late stages of the D_e deformation almost parallel to the L_e stretching lineation may be related to the transpressional field that developed during strike-slip movements, recognized in the whole SRB area and/or to a constrictional strain developed during the D_e progression (shortening in the Y-axis of the D_e strain ellipsoid; Fig. 11).

For the time span between the Late Cretaceous and the Eocene we have no good evidence for the structural evolution of the study area. This can be attributed to the fact that relevant structures formed during this time interval were strongly overprinted by the younger Tertiary deformational events. However, Burchfiel (1980) recognized contractional SW-vergent structures along the eastern parts of the Apulia fragment and eastward contractional structures along the eastern margin of the Rhodope fragment, related to an initial collisional stage during Late Cretaceous to Paleocene times between the Rhodope (including SRB) and the Apulia fragments. He also mentioned continued convergence between both fragments during Eocene–Oligocene times, when the Eocene blueschist belt formation and the main collision took place, due to an A-type subduction (Schermer 1990).

We speculate that some of the low-angle southwestward thrust faults and the subsequent northeastward back-thrusting mentioned by Echtler et al. (1987) belong (according to their description) to the initial Late Cretaceous to Paleocene convergent event between the SRB/Rhodopian and Apulia fragments. The Late Oligocene–Miocene southwestward brittle thrust zones, described here at the western SRB marginal parts and the Circum-Rhodope belt, are unambiguously younger compressional structures. These local structures are possibly related to the Oligocene–Miocene downward to SW detachment of the SRB hangingwall, described by Dinter and Royden (1993) and Sokoutis et al. (1993), forming gravity-driven thrusts (Fig. 11).

Discussion and conclusions

We have shown that NE–SW subhorizontal extension affected the SRB metamorhpic rocks during the Eocene associated with tectonic unroofing of the SRB and the upper Rhodope Sidironero unit. Tectonic denudation took place along the D_e low-angle shear zones which merged into the Eocene amphibolite facies shear zones of Sidironero unit in the footwall (Fig. 10b).

The mid-Oligocene Xanthi pluton that intruded into the Sidironero metamorphic rocks and exhibits no ductile deformation (Meyer 1968; Liati 1986) shows that the ductile deformation of the Sidironero unit ended before the Middle Oligocene. Like the Sidironero unit, the SRB stopped deforming ductilely before the Middle Oligocene.

Where the Rhodope Pangaio unit was located during the Eocene is still an unanswered question. In any case, during the Oligocene–Miocene the Pangaio unit was beneath the cold Sidironero and SRB, influenced by an upper greenschist facies metamorphism associated with southwestward extensional shearing (Kilias and Mountrakis 1990; Kolocotroni and Dixon 1991; Wawrzenitz et al. 1995; Dinter et al. 1995). Northeast/southwest extension continued during the whole Oligocene–Miocene period, ductile at depth and brittle in the SRB und Sidironero upper crustal levels, presently causing the unroofing of the Pangaio unit that was finally juxtaposed to the SRB upper plate (Fig. 10d). The oldest Middle–Late Miocene sediments (Xidas 1984) of the tectonic basins on the Pangaio unit mark the exhumation time of this unit.

The structural evolution of the SRB/Rhodope metamorphic province indicates that during Tertiary times the whole SRB/Rhodope metamorphic pile underwent successive extensional unroofing and exhumation. From rim to core of this metamorphic pile, a progressively younger age for the metamorphic peak is observed from Eocene to Early Miocene, as well as a time delay in the exhumation of the tectonically deeper parts of the core relative to the overlying parts of the rim (Fig. 10e). Therefore, in the Hellenic hinterland of northern Greece a NE–SW crustal stretching associated with crustal exhumation was initiated in the latest Eocene. In contrast, in the Cyclades and Olympos–Ossa areas, a NNE/SSW to NE/SW-oriented crustal-scale extension and exhumation initially took place during Oligocene–Miocene times (Lister et al. 1984; Schermer 1990, 1993; Kilias et al. 1991; Buick 1991; Gautier et al. 1993). Even more externally, in Crete, Kilias et al. (1994) and Fassoulas et al. (1994) demonstrated a N/S-directed extension associated with deep crustal uplift from the Middle Miocene. As a consequence, a progressive migration of crustal stretching and associated uplifting toward SSW during Tertiary times, from the Hellenic hinterland to the external Hellenides, can be concluded (Fig. 12).

The migration of extension was associated with contemporaneous SSW migration of compression until the present position at the active NE-dipping Hellenic subduction zone. The migration of compression is shown by the two high-pressure/low-temperature metamorphic belts of Eocene and Late Oligocene/Early Miocene age (Fig. 12), as well as the continuous age decrease of the associated thrust belt toward the more external Hellenides (Godfriaux 1968; Andriessen et al. 1979; Seidel et al. 1982; Schliestedt et al. 1987; Schermer et al. 1989; Schermer 1990; Kilias et al. 1991, 1994). High-pressure/low-temperature metamorphism and compression are related to successive, SW-

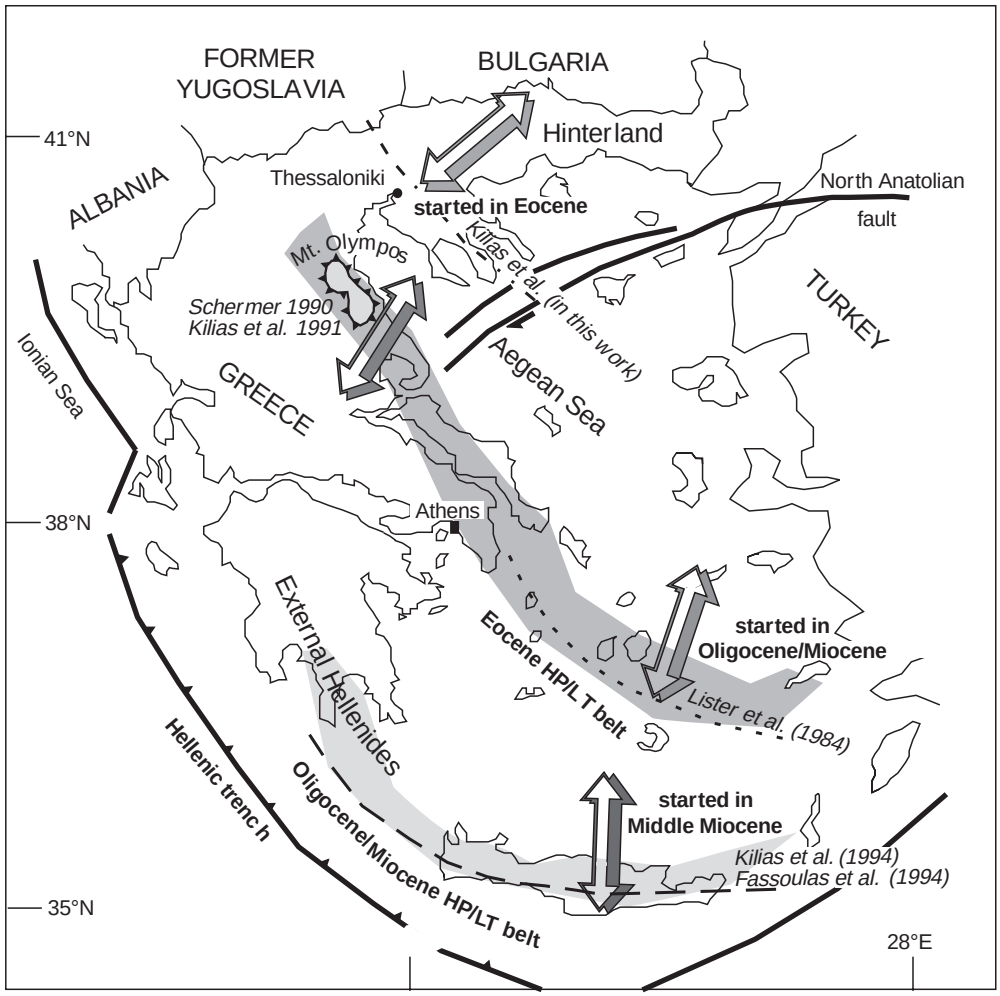

Fig. 12 The southwestward progressive migration during Tertiary times of the maximum extension from the Hellenic hinterland toward the external Hellenides. The ages correspond to the initiation of the extension in the specific areas of the Hellenic orogen

migrating subduction processes during Tertiary plate convergence (Seidel et al. 1982; Lister et al. 1984; Schermer 1990; Fassoulas et al. 1994). Therefore, in the Hellenides, tertiary extension and compression, associated with plate convergence, form a south/southwestward migrating system. In each case compression is followed by extension. The deeper crustal parts were exhumed and stretched simultaneously with underplating and stacking of new material at the front.

The Middle–Late Cretaceous deformation of the SRB represents an older ductile tectonic event, probably associated with a subhorizontal crustal stretching and crustal unroofing. This took place behind the thrust belt that developed at the northern Rhodope border, during the Cretaceous continent–continent collision between the Rhodope (SRB included) and Moesian fragments.

Appendix

Fault size and attitude, fault-striae orientation, sense of slip and polyphase slip and its relative chronology were measured and determined in the field. Fault size is classified qualitatively based on an estimation of the displacement and the lateral extent of the fault. The aim was to discriminate first-order faults. Striae orientation and relative slip chronology enable, in favourable cases, the discrimination of superposed palaeostress states. Faults were considered to be temporarily related if the following criteria were satisfied: (a) geometrically compatible movement senses, including the possibility of conjugate pairs (Krantz 1988); (b) similar fault surface mineral assemblages when the faults occurred in similar host lithologies; and (c) relative fault ages similar to other distinct features.

All methods to derive palaeostress tensor configurations assume: (a) a homogeneous stress field; (b) slip occurs in the direction of maximum resolved shear stress in the fault plane, which is parallel to the measured slickenline; and (c) fault displacements are small relative to fault surface area.

The "pressure–tension (P–T) axes method" (Turner 1953; the method was originally devised for calcite twinning) places σ_1 30° (as an empirical value) from the fault plane in the plane defined by the pole to the fault plane and the striae, in such a way as to cause movement in the direction recorded for each fault. The σ_3 is

placed 90° from σ_1. A conditioned least-squares fit is used to locate mean σ_1 to σ_3 orientations.

The "grid search method" (Gephart and Forsyth 1984) tests thousands of tensors against the fault data and selects all possible tensors that best fit all or portions of the data. Fit is accepted if the angular divergence between predicted and recorded slip directions is less than 20° and if the resolved coefficient of friction (μ) on the fault surface is greater than 0.4 (from laboratory experiments the (μ) value ranges from 0.6 to 0.9; Byerlee 1968). A tensor is considered acceptable if 20% or more of the data fit within these limits.

Acknowledgements We are grateful to W. Frisch and U. Ring for discussions and helpful criticism of the manuscript. We also thank L. Ratschbacher, S. Wallis and an anonymous referee for careful review, and W.C. Dullo and C. Simpson for editorial assistance.

References

Altherr R, Schliestedt M, Okrusch M, Seidel E, Kreuzer H, Harre W, Lenz H, Wendt I, Wagner G (1979) Geochronology of high-pressure rocks on Sifnos (Greece, Cyclades). Contrib Mineral Petrol 70:245–255

Andriessen PA, Boelruk NA, Herbeda EH, Priem HM, Verdurmen EA, Verschure RH (1979) Dating the events of metamorphism and granitic magmatism in the Alpine Orogen at Naxos (Cyclades, Greece). Contrib Mineral Petrol 69:215–225

Blake MC, Bonneau M, Geyssant J, Kienast JR, Lepvier C, Maluski H, Papanikolaou D (1981) A geological reconnaissance of the Cycladic blueschist belt, Greece. Geol Soc Am Bull 92:247–254

Bonèev E (1966) Revue génerale de la structure géologique de la Bulgaria. Bull Geol Inst 15:5–24

Bonèev E (1971) Problems of the Bulgarian geotectonics. Technica 204 pp (in Bulgarian)

Bonèev E (1988) Notes sur la téctonique alpine des Balkans. Bull Soc Géol France 8:241–249

Borsi S, Ferrara G, Mercier J (1965) Détermination de l' age des séries métamorphiques du Massif Serbomacédonien au Nord-Est de Thessalonique (Grèce) par les methodes Rb/Sr et K/Ar. Ann Soc Géol Nord 84:223–225

Buick IS (1991) The late Alpine evolution of an extensional shear zone, Naxos, Greece. J Geol Soc Lond 148:93–103

Burchfiel BC (1980) Eastern European alpine system and the Carpathian orocline as an example of collision tectonics. Tectonophysics 63:31–61

Burg JP, Ivanov Z, Ricou LE, Dimov D, Klain L (1990) Implications of shear-sense criteria for the tectonic evolution of the Central Rhodope Massif, southern Bulgaria. Geology 18:451–454

Burg JP, Godfriaux I, Ricou LE (1995) Extension of the Mesozoic Rhodope thrust units in the Vertiskos-Kerdilion Massifs (northern Greece). C R Acad Paris 320:889–896

Burg JP, Ricou LE, Ivanov Z, Godfriaux I, Dimov D, Klain L (1996) Syn-metamorphic nappe complex in the Rhodope Massif. Structures and kinematics. Terra Nova 8:6–15

Byerlee JD (1968) Brittle–ductile transition in rocks. J Geophys Res 73:4741–4750

Chatzidimitriadis E, Kilias A, Staikopoulos G (1985) Nouvi aspetti petrologici e tettonici del massiccio Serbomacedonne e delle regioni adiacenti, della Grecia del Nortd. Boll Soc Geol It 104:515–526

Christofides G, D'Amico C, Del Moro A, Eleftheriades G, Kyriakopoulos C (1990) Rb/Sr geochronology and geochemical characters of the Sithonia plutonic complex (Greece). Eur J Mineral 2:79–87

D'Amico C, Christofides G, Eleftheriades G, Bargossi G, Campana R, Soldatos T (1991) The Sithonia Plutonic Complex (Chalkidiki, Greece). Mineral Petrogr Acta 33:143–177

De Wet AP, Miller JA, Bickle MJ, Chapman HJ (1989) Geology and geochronology of the Arnea, Sithonia and Ouranoupolis intrusions, Chalkidiki peninsula, northern Greece. Tectonophysics 161:65–79

Dercourt J, Ricou LE, Vrielynck B (1993) Atlas tethys palaeoenvironmental Maps. Gauthier-Villars, Paris

Dimitriadis S, Godelitsas A (1991) Evidence for high pressure metamorphism in the Vertiskos group of the Serbomacedonian massif. The eclogite of Nea Roda, Chalkidiki. Bull Geol Soc Greece 25:67–80

Dimitrijeviè D (1974) Sur l' age du métamorphisme et des plissements dans la masse Serbomacédonienne. Bull VI Congr Assoc Geol Carpatho-Balcanique 1:339–347

Dimitrijeviè M, Ciriè B (1966) Der tektonische Bau des Serbomazedonischen Massivs. Geotectonica 5:32–41

Dinter DA (1994) Tectonic evolution of the Rhodope metamorphic core complex, northern Greece. PhD thesis, MIT, Cambridge, 320 pp

Dinter DA, Royden L (1993) Late Cenozoic extension in northeastern Greece: Strymon Valley detachment system and Rhodope metamorphic core complex. Geology 21:45–48

Dinter DA, Macfarlane A, Hames W, Isachsen C, Bowring S, Royden L (1995) U–Pb and $^{40}Ar/^{39}Ar$ geochronology of the Symvolon granodiorite: implications for the thermal and structural evolution of the Rhodope metamorphic core complex, northeastern Greece. Tectonics 14:886–908

Dixon JE, Dimitriadis S (1984) Metamorphosed ophiolitic rocks from the Serbo-Macedonian Massif, near Lake Volvi, Northeast Greece. Geol Soc Lond Spec Publ 17:603–618

Dürr S, Altherr R, Keller J, Okrusch M, Seidel E (1978) The median Aegean Crystalline Belt: stratigraphy, structure, metamorphism, magmatism. IUCG Sci Rep. 38:455–477

Echtler H, Matte P, Maluski H (1987) Large southwestward ductile thrusting in the alpine Serbomacedonian belt. Terra Cogn 7:106

Fassoulas C, Kilias A, Mountrakis D (1994) Postnappe stacking extension and exhumation of high-pressure/low-temperature rocks in the island of Crete, Greece. Tectonics 13:127–138

Ferry JM, Spear FS (1978) Experimental calibration of the partitioning of the Fe and Mg between biotite and garnet. Contrib Mineral Petrol 66:113–117

Gautier P, Brun JP, Jolivet L (1993) Structure and kinematics of upper Cenozoic extensional detachment on Naxos and Paros (Cyclades islands, Greece). Tectonics 12:1180–1194

Ghosh SK, Ramberg H (1976) Reorientation of inclusions by combination of pure shear and simple shear. Tectonophysics 34:1–70

Gephart JW, Forsyth DW (1984) An improved method for determining the regional stress tensor using earthquake focal mechanism data: application to the San Fernando earthquake sequence. J Geophys Res 89:9305–9320

Godfriaux I (1968) Etude géologique de la région de l'Olympe (Grèce). Ann Géol Pays Héll 19:1–280

Hancock M (1985) Brittle microtectonics: principles and practice. J Struct Geol 7:437–457

Hanmer S, Passchier C (1991) Shear-sense indicators: a review. Geol Surv Can Pap M44–90/17 E, 72 pp

Hoisch DT (1989) A muscovite–biotite geothermometer. Am Mineral 74:565–572

Hynes A, Forest RC (1988) Empirical garnet–muscovite geothermometry in low grade metapelites, Selwyn Range (Canadian Rockies). J Metamorph Geol 6:297–309

Ivanov Z (1988) Apercu géneral sur l' évolution géologique et structurale du massif des Rhodopes dans le cadre des Balkanides. Bull Soc Géol France 8:227–240

Jacobshagen V, Dürr S, Kockel F, Kopp KO, Kowalczyk G, Berckhemer H, Bûttner D (1978) Structure and geodynamic evolution of the Aegean region. In: Closs H, Roeder D, Schmidt K (eds) Alps, Apennines, Hellenides. Schweizerbart, Stuttgart, pp 537–564

Jones EC, Tarney J, Baker JH, Gerouki F (1992) Tertiary granitoids of Rhodope, northern Greece: magmatism related to extensional collapse of the Hellenic Orogen? Tectonophysics 210:295–314

Karfakis J, Doutsos T (1995) Late orogenic evolution of the Circum-Rhodope Belt, Greece. N Jahrb Geol Paläont Mh 5:305–319

Kassoli-Fournaraki A (1981) Contribution to the mineralogical and petrological study of amphibolitic rocks from the Serbomacedonian massif. PhD thesis, Univ Thessaloniki, 231 pp (in Greek)

Katsikatsos G (1977) La structure téctonique d'Attique et de l'ile d'Eubee. In: Kallergis G (ed) Sixth colloquium on the geology of the Aegean region, Athens, pp 211–228

Kauffman G, Kockel F, Mollat H (1976) Notes on the stratigraphic and paleogeographic position of the Svoula formation in the innermost zone of the Hellenides (northern Greece). Bull Soc Geol France 18:225–230

Kilias A, Mountrakis D (1990) Kinematics of the crystalline sequences in the western Rhodope massif. Geol Rhodop 2:100–116

Kilias A, Frisch W, Ratschbacher L, Sfeikos A (1991) Structural evolution and P/T conditions of metamorphism of blue schists of E. Thessaly. Bull Geol Soc Greece 25:81–99

Kilias A, Fassoulas C, Mountrakis D (1994) Tertiary extension of continental crust and uplift of Psiloritis metamorphic core complex in the central part of the Hellenic arc (Crete, Greece). Geol Rundsch 83:417–430

Kockel F, Walther H (1965) Die Strimonlinie als Grenze zwischen Serbo-Mazedonischem und Rila-Rhodope Massiv in Ost Mazedonien. Geol Jahrb 83:575–602

Kockel F, Mollat H, Walther H (1971) Geologie des Serbomazedonischen Massivs und seines mesozoischen Rahmes (Nordgrienchenland). Geol Jahrb 89:529–551

Kockel F, Mollat H, Walther H (1977) Erläuterungen zur geologischen Karte der Chalkidhiki und angrenzender Gebiete, 1:100,000 (Nord-Griechenland). Bundesanstalt fur Geowisseschaften und Rohstoffe, Hannover, 119 pp

Kohn MJ, Spear F (1989) Empirical calibration of geobarometers for the assemblage garnet + hornblende + plagioclase + quartz. Am Mineral 74:77–84

Kolocotroni C, Dixon JE (1991) The origin and emplacement of the Vrontou granite, Serres, NE Greece. Bull Geol Soc Greece 25:469–483

Koukouzas C (1972) Le chévauchement de Strymon dans la région de la frontiere Grecobulgare. Z Dtsch Geol Gesell 123:343–348

Kourou A (1991) Lithology, tectonic, geochemistry and metamorphism in the western part of Vertiskos group. The area NE from the lake Agios Vasilios, northern Greece. PhD thesis, Univ Thessaloniki, 461 pp (in Greek)

Krantz RW (1988) Multiple fault sets and tree dimensional strain: theory and application. J Struct Geol 10:225–237

Kronberg P, Eltgen H (1971) Geological map of Greece; Xanthi sheet, scale 1:50,000. IGME, Athens

Kronberg P, Meyer W, Pilger A (1970) Geologie der Rila-Rhodope Masse zwischen Strimon und Nestos (Nordgriechenland). Beih Geol Jahrb 88:133–180

Laird J, Lanphere MA, Albee AL (1984) Distribution of Ordovician and Devonian metamorphism in mafic and pelitic schists from northern Vermont. Am J Sci 284:376–413

Lee J, Lister GS (1992) Late Miocene ductile extension and detachment faulting, Mykonos, Greece. Geology 20:121–124

Liati A (1986) Regional metamorphism and overprinting contact metamorphism of the Rhodope zone, near Xanthi (N. Greece): petrology, geochemistry, geochronology. PhD thesis, Technical Univ Braunschweig, 186 pp

Lister GS, Davis GA (1989) The origin of metamorphic core complexes and detachment faults formed during Tertiary continental extension in the northern Colorado River region, U.S.A. J Struct Geol 11:65–94

Lister GS, Banca G, Feenstra A (1984) Metamorphic core complexes of Cordilleran type in the Cyclades, Aegean Sea, Greece. Geology 12:221–225

Massonne JH, Schreyer W (1987) Phengite geobarometry based on the limiting assemblage with K-feldspar, phlogopite and quartz. Contrib Mineral Petrol 96:212–224

Mercier JL (1968) Etude géologique des zones internes des Héllénides en Macédoine centrale (Grèce). Contribution a l'étude du métamorphisme et de l'évolution magmatique des zone internes des Héllénides. Ann Géol Pays Héll 20:1–792

Mercier JL, Vergely P, Bebien J (1975) Les ophiolites héllèniques "obductees" au Jurassique superieur sont-elles les vestiges d'une mer marginale peri-europeenne. C R Somm Soc Géol France 17:108–122

Meyer W (1968) Zur Alterstellung des Plutonismus im Südteil der Rila-Rhodope-Masse (Nordgriechenland). Geol Paläont 2:173–192

Mposkos E, Liati A, Katagas C, Arvanitides N (1990) Petrology of the metamorphic rocks of western Rhodope, Drama area, N. Greece. Geol Rhodop 2:127–142

Nachev IK (1993) Late Cretaceous paleogeodynamics of Bulgaria. Geol Balc 23:3–23

Nasir S (1994) PtOXY: software package for the calculation of pressure–temperature oxygen fugacity using a selection of metamorphic geothermobarometers. Comput Geosci 20:1297–1320

Papadakis A (1971) On the age of the granitic intrusion near Stratonion, Chalkidiki (Greece). Ann Geol Pays Héll 23:297–300

Papadopoulos P (1982) Geological map of Greece; Maronia sheet, scale 1:50,000. IGME, Athens

Papadopoulos C, Kilias A (1985) Altersbeziehungen zwischen Metamorphose und Deformation im zentralen Teil des Serbomazedonischen Massivs (Vertiskos Gebirge, Nord-Griechenland). Geol Rundsch 74:77–85

Papanikolaou D, Panagopoulos A (1981) On the structural style of southern Rhodope, Greece. Geol Balc 11:13–22

Passchier CW (1987) Stable positions of rigid objects in noncoaxial flow: a study in vorticity analysis. J Struct Geol 9:679–690

Pavlides SB, Kilias AA (1987) Neotectonic and active faults along the Serbomacedonian zone (SE Chalkidiki, northern Greece). Ann Tecton 1:97–104

Plyusnina LP (1982) Geothermometry and geobarometry of plagioclase–hornblende bearing assemblages. Contrib Mineral Petrol 80:140–146

Powell R, Holland TJB (1990) Calculated mineral equilibria in the pelite system, KFMASH (K_2O–FeO–MgO–Al_2O_3–SiO_2–H_2O). Am Mineral 75:367–380

Psilovikos A (1977) Palaeogeographical evolution of the Mygdonia basin and lake (Langada-Volvi). PhD thesis, Univ Thessaloniki, 156 pp (in Greek)

Ratschbacher L, Frisch, W, Neubauer F, Schmid SM, Neugebauer J (1989) Extension in compressional orogenic belts: the eastern Alps. Geology 17:404–407

Ratschbacher L, Riller U, Meschede M, Herrman U, Frisch W (1991) Second look at suspect terranes in southern Mexico. Geology 19:1233–1236

Ricou LE (1994) Tethys reconstructed: plates, continental fragments and their boundaries since 260 Ma from Central America to South-eastern Asia. Geodyn Acta 7:169–218

Roussos N (1995) Stratigraphy and paleogeographic evolution of the Paleogene molassic basins of the north Aegean area. Bull Geol Soc Greece 30:275–294

Sakellariou D (1989) The geology of the Serbomacedonian massif in the northeastern Chalkidiki peninsula, North Greece. Deformation and metamorphism. PhD thesis, Univ Mainz, 177 pp

Sapountzis SE, Soldatos K, Eleftheriades G, Christofides G (1976) Contribution to the study of the Sithonia plutonic complex (N. Greece). II. Petrography, petrogenesis. Ann Geol Pays Héll 28:99–134

Schermer ER (1990) Mechanisms of blueschist creation and preservation in an A-type subduction zone, Mount Olympos region, Greece. Geology 18:1130–1133

Schermer ER (1993) Geometry and kinematics of continental basement deformation during the Alpine orogeny, Mt. Olympos region, Greece. J Struct Geol 15:571–591

Schermer E, Lux D, Burchfiel B (1989) Age and tectonic significance of metamorphic events in the Mt. Olympos region (Greece). Bull Geol Soc Greece 23:13–27

Schliestedt M, Altherr R, Matthews A (1987) Evolution of the Cycladic crystalline complex: petrology, isotope geochemistry and geochronology. In: Helgeson HC (ed) Chemical transport in metasomatic processes. Reidel, Dordrecht, pp 389–428

Schreurs J (1985) Prograde metamorphism of metapelites, garnet–biotite thermometry and prograde changes of biotite chemistry in high-grade rocks of west Unsimaa, southwest Finland. Lithos 18:69–80

Seidel E, Kreuzer H, Harre W (1982) A Late Oligocene/Early Miocene high pressure belt in the external Hellenides. Geol Jahrb E23:165–206

Sengör AMC, Yilmaz Y, Sungurlu O (1984) Tectonics of the Mediterranean Cimmerides: nature and evolution of the western termination of Paleo-Tethys. Geol Soc Lond Spec Publ 17:77–112

Sidiropoulos N (1991) Lithology, geochemistry, tectonic and metamorphism of the Disoro mountain area (northwestern part of Vertiskos unit, North Greece). PhD thesis, Univ Thessaloniki, 586 pp (in Greek)

Simpson C, Schmid SM (1983) An evaluation of criteria to deduce the sense of movement in sheared rocks. Geol Soc Am Bull 94:1281–1288

Sokoutis D, Brun JP, Van den Driessche J, Pavlides S (1993) A major Oligocene–Miocene detachment in southern Rhodope controlling north Aegean extension. J Geol Soc Lond 150:243–246

Spassov CS (1961) Notizen über die Palaeogeographie und tecktonische Aktivität während des Palaeozoikums. Trav Geol Bulg Ser Strat Tect 2:43–54 (in Bulgarian)

Spear FS, Rumble D (1986) Pressure, temperature and structural evolution of the Oxfordville Belt, West-Central New Hampshire. J Petrol 27:1071–1093

Spear FS, Hickmott DD, Selverstone J (1990) Metamorphic consequences of thrust emplacement, Fall Mountain, New Hampshire. Geol Soc Am Bull 102:1344–1360

Tranos DM, Kilias AA, Mountrakis MD (1993) Emplacement and deformation of the Sithonia granitoid pluton (Macedonia, Greece). Bull Geol Soc Greece 28:195–211

Turner F (1953) Nature and dynamic interpretation of deformation lamellae in calcite of three marbles. Am J Sci 4:276–298

Vergely P (1984) Téctonique des ophiolites dans les Héllénides Internes (déformations, métamorphismes et phénoménes sédimentaires). Conséquences sur l'évolution des régions Téthysiennes Occidentales. These Doct. d'Etat, Paris-Sud, 650 pp

Wallis SR, Platt JP, Knott SD (1993) Recognition of synconvergence extension in accretionary wedges with examples from the Calabrian arc and the Eastern Alps. Am J Sci 293:463–495

Wawrzenitz N, Baumann A, Nollau G (1995) Miocene uplift of mid-crustal rocks in the Rhodope Metamorphic Core Complex, caused by late alpine extension of previously thickened crust (Thassos Island, Pangaeon Complex, Northern Greece). Bull Geol Soc Greece 30:147–157

Wernicke BP (1981) Low-angle normal faults in the Basin and Range Province: nappe tectonics in an extending orogen. Nature 291:645–648

Xidas S (1984) Geological map of Greece; Rhodolivos sheet, scale 1:50,000. IGME, Athens

Zachos S, Dimadis E (1983) The geotectonic position of the Skaloti-Echinos granite and its relationship to the metamorphic formations of Greek Western and Central Rhodope. Geol Balc 13:17–24

Zagorcev I (1992) Neotectonic development of the Strumna (Kraistid) Lineament, southwest Bulgaria and northern Greece. Geol Mag 129:197–222